Ph.D. in Electronic and Computer Engineering
Dept. of Electrical and Electronic Engineering
University of Cagliari

Algorithms for the synchrophasor measurement in steady-state and dynamic conditions

Paolo Castello

Advisor: Prof. Carlo Muscas

Curriculum: ING-INF/07 Misure Elettriche Elettroniche

XXVI Cycle

March 2014

I dedicate this work to my Family, especially to my brother Eugenio

Contents

Abstract 6
Introduction 8
1 Synchrophasors and Phasor Measurement Units 12
1.1 The standard of synchrophasor IEEE C37.118.1-2011 12
1.2 General structure of Phasor Measurement Units 13
1.2.1 Local time dissemination 15
1.3 The definition of synchrophasor, frequency and ROCOF 16
1.3.1 Synchrophasor definition 16
1.3.2 Frequency and ROCOF definitions 18
1.4 Measurement evaluations 19
1.4.1 TVE 19
1.4.2 Frequency Error and ROCOF error 21
1.4.3 Indices for step tests 22
1.4.4 The latency 23
1.5 Measurement compliance tests 24
1.5.1 Steady state compliance 24
1.5.2 Dynamic compliance 26
1.5.3 Step change 27
1.6 Other standards of interests in synchrophasor measurement 28
1.6.1 IEEE C37.118.2-2011 28
1.6.2 IEEE C37.242-2013 28
1.6.3 IEC 61850-90-5 29
2 Algorithms for synchrophasor estimation 31
2.1 The sources of uncertainty 31
2.2 The synchrophasor estimation 34
2.2.1 The general model 35
2.3 The steady state algorithms 36
2.4 The dynamic algorithms 37
2.4.1 The algorithm TFT-WLS 38
2.5 The test cases for the comparison of the different algorithms 39
2.5.1 Steady-state tests 40
2.5.2 Dynamic tests 41
2.6 The tests system 42
2.7 The test results 43
2.7.1 Noise 43

2.7.2 Off-nominal frequencies 43
2.7.3 Harmonics 43
2.7.4 Interharmonics 45
2.7.5 Modulation 45
2.7.6 Ramp tests 47
2.7.7 Step tests 48
2.7.8 Final considerations 49
3 Proposals to improve the performance in the synchrophasor estimation 51
3.1 Fast response to changing conditions 51
3.1.1 Proposed algorithm modification 52
3.1.2 The tests of the proposed solution 54
3.2 The P+M synchrophasor methods 58
3.2.1 The tests of the proposed solution 61
3.3 A PMU for electrical distribution networks 67
4 A distributed PMU for the electrical substations 75
4.1 The distributed PMU 75
4.1.1 The standard IEC 61850 76
4.1.2 The standard IEEE 1588-2008 77
4.1.3 A distributed measurement network based on IEC 61850 77
4.1.4 The test setup 79
4.1.5 Test results 79
Conclusions 88
Publications 90
Bibliography 91
Acknowledgements 94
List of figures 96
List of tables 98

Abstract

Phasor measurement units (PMUs) are becoming one of the key issues of power network monitoring. They have to be able to perform accurate estimations of current and voltage signals either under steady-state or dynamic conditions.

The first part of this PhD thesis analyses the impact of the phasor models on the estimation accuracy, focuses on algorithms proposed in the literature for the estimation of phasors and studies their performance under several different conditions.

On the basis of the results of this analysis, in the second part of this thesis an innovative approach to improve the performance of synchrophasor estimation is presented. The method proposes a modified version of the synchrophasor estimation algorithm which uses the non-orthogonal transform defined as Taylor-Fourier Transform (TFT) and which is based on a Weighted Least Squares (WLS) estimation of the parameters of a second order Taylor model of the phasor. The aim of the proposed enhancements is to improve the performance of the algorithm in presence of fast transient events and to achieve a Phasor Measurement Unit that is simultaneously compliant with both M and P compliance classes, suggested by the synchrophasor standard IEEE C37.118.1. In particular, while the TFT based adaptive algorithm is used for synchrophasor estimation, frequency and Rate of Change of Frequency (ROCOF) are estimated using the higher derivatives outputs of the adaptive TFT. Frequency estimation feedback is used to tune the algorithm and achieve better performance in off-nominal conditions. The proposed approaches are validated by means of simulations in all the static and dynamic conditions defined in the standard.

In the last chapter, the algorithm proposed above is used in a novel architecture, compliant to IEC 61850, for a distributed IED-based PMU, to be used in electrical substations. In particular, a measurement architecture based on process bus and sampled values synchronized with IEEE 1588-2008 is proposed, so that voltage and current signals are acquired by a Merging Unit device, while the PMU signal processing is performed on a IED (Intelligent Electronic Device), in compliance with IEEE C37.118.1-2011.

Introduction

In the last few years the importance of Wide Area Measurement Systems (WAMSs) has been increasing for the control and the management of electric networks, also due to the growth of energy generation from renewable sources. The necessity to know how the electrical quantities change from different and distant points of the electrical transmission networks asks for the development of new measurement instrumentation.

The Phasor Measurement Unit (PMU) is the key element of the WAMS that permits the measurement of the electric quantities of interest (voltage and current phasors, frequency and rate of change of frequency). PMUs also allow the synchronization and the transmission of the performed measurements. The PMUs are described in the Standard IEEE C37.118 about synchrophasor measurement in electric power systems.

Nowadays, there are different vendors of PMUs and the number of devices in the electrical network is constantly increasing. Thus, one of the most important issues in WAMS is the interoperability of the commercial PMUs. If the interoperability is not respected, a generic electric phenomenon could be evaluated differently from two PMUs. The different evaluation of the same event could even trigger an involuntary protection action in the electric system. One of the reasons that influence the interoperability is the algorithm implemented in the PMU.

The standard does not suggest one algorithm, but specifies the accuracy limits of the measurement for different tests. In scientific literature, there are different algorithms for synchrophasor estimation, but it is difficult to compare their performance without a standard index. For the evaluation, only one index is present in the standard IEEE C37.118 2005: the Total Vector Error (TVE) that represents the absolute value of the relative vector difference between the real and measured phasor. With the release of the IEEE standard C37.118.1-2011, different indices are presented to evaluate the accuracy of a synchrophasor measurement in different scenarios and new improved definitions about the dynamic synchrophasor, frequency and rate of change of frequency (ROCOF) measurement are introduced.

Different algorithms rely on different mathematic model. The most common model is the steady state model, where the acquired electric signal is considered stationary during the observation period and is thus described by magnitude and phase, along with actual frequency. On the other hand, in order to better represent the non-stationary signals that are actually present

in power grids, a more suitable approach is to consider a dynamic model, which describes the magnitude and phase as functions of time in the acquisition window.

The first part of this thesis aims at evaluating the performance of different algorithms proposed in the literature for synchrophasor measurement, under both steady state and dynamic conditions. The results of these tests will allow advantages and drawbacks of each approach to be identified.

Starting from these outcomes, in the second part of the thesis an innovative approach is proposed to improve the performance of the studied algorithms. In particular, by considering that the best performance are achieved by a dynamic algorithm that uses the Weight Least Squares and the second order Taylor Fourier Transform, in the following referred to as TF-WLS, and that the main limit of this approach is represented by high response time in presence of rapid step changes, an adaptive version of this method is proposed. In short, in the modified method the possible presence of rapid dynamic events is detected, thus allowing the algorithm to adapt the length and the weights of the acquisition window, in order to have a faster response to these events. Different implementations of this general approach are described, with successive improvements. The final goal is defining an algorithm that complies simultaneously with the requirements of the two different performance classes introduced by the standard IEEE C37.118.1-2011.

The practical feasibility of the proposed approach has been tested with a prototype PMU specifically designed for electric distribution networks. The design of the prototype had two main, somewhat contrasting, requirements: a low cost per unit, because the electric distribution network needs a large number of measurement devices; a high measurement accuracy, in particular for the phase angle, because in the electrical distribution networks the angle differences are smaller compared to the electrical transmission networks. The process and the choices adopted to create the prototype are described and discussed in chapter 3

In the last chapter, the proposed algorithms for synchrophasor evaluation are implemented in an innovative approach aimed at defining a distributed PMU for an electric substation, where the communications comply with the standards IEC 61850. Indeed, while the traditional PMUs are standalone devices, the new standards permit to consider a distributed architecture, where the different functionalities (acquisition, synchronization, communication, etc.) are performed by different devices spread in different areas of the electric substations. Inevitably, the new architecture needs new tests to verify the synchronization through the different parts of the system

and consequently the accuracy of the measurements. For this reason, the algorithm, which was originally designed for a standalone PMU, has been tested in this new scenario, providing positive results and thus showing the feasibility of the distributed approach.

1 Synchrophasors and Phasor Measurement Units

1.1 The standard of synchrophasor IEEE C37.118.1-2011

The original synchrophasor standard was IEEE Std 1344-1995. It was replaced by IEEE Std C37.118-2005 and the new version of the 2011 is divided into two standards: IEEE Std C37.118.1-2011, in the following called "the synchrophasor standard", covering measurement provisions, and IEEE C37.118.2-2011, covering data communication.

In the new synchrophasor standard, the phasor and synchronized phasor definitions, as well as the concepts of total vector error (TVE) are presented and also the important dynamic performance tests have been introduced along with other indices used to evaluate the new compliance tests. In addition, measurement of frequency and rate of change of frequency (ROCOF) have been regulated.

The PMUs are used in many protection and data acquisition functions in transmission and distribution electrical networks. The PMU refers the measurements to a common time base, generally the Universal Coordinated Time (UTC) obtained from the Global Position Systems (GPS). In this way the measurements become comparable over a wide area. A synchrophasor is a phasor value obtained from voltage or current signals and referenced to a common time base.

The goal of PMU devices connected to the power grid is to monitor power system parameters and to track power system dynamic phenomena for improved power system monitoring, protection, operation, and control. The intent of the synchrophasor standard is to describe and quantify the performance of the PMU deployed to monitor the power grid. The PMU measures the magnitude, phase angle, frequency, and ROCOF from the voltage and current signals. These signals may be corrupted by distortion, noise, and abrupt changes caused by system loads, control and protective actions. These different disturbs complicate the process of measuring.

The standard defines two classes of performance: P class and M class. P class is specific for protection applications requiring fast response. M class is specific for measurement application and is intended for applications that could be adversely effected by aliased signals and do not require the fastest reporting speed. All the compliance tests are specified by performance of P and M class.

In most cases, the frequency and ROCOF are computed as the first derivative and the second derivative of the estimated synchrophasor phase angle. These two quantities are less reliable measurements, particularly ROCOF, because they are more sensitive to disturbances and noise.

The PMU shall support data reporting or reporting rate at sub-multiples of the nominal system frequency. Required reporting rate (Fs, Frames per second) for 50 Hz and 60 Hz systems are listed in the Table 1. Other reporting rates are permissible, and including higher rates like 100 frames/s or 120 frames/s or rates lower than 10 frames/s, such as 1 frames/s, is encouraged.

Table 1. Required PMU reporting rate.

System Frequency	**50 Hz**			**60 Hz**					
Fs	10	25	50	10	12	15	20	30	60

In the synchrophasor standard different tests are presented, both in steady state and in dynamic conditions, to ensure that compliant instruments will perform similarly when they meet similar conditions.

1.2 General structure of Phasor Measurement Units

Phasor Measurement Units or PMUs are a key element of the Wide Area Measurement Systems (WAMS). The PMU is a device that provides synchronized phasor measurements of voltage and current. The PMU, an example of which is shown in Figure 1, is a standalone device but it is possible to integrate the function of the synchronized phasor measurement into an IED (Intelligent Electronic Device).

Figure 1. Standalone PMU device from Arbiter, model 1133A power sentinel.

A PMU device is composed by different elements, as shown in Figure 2:

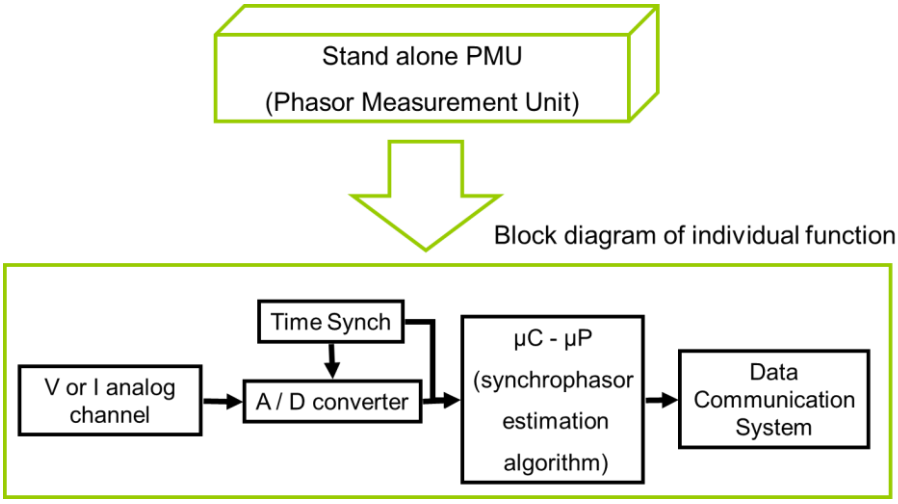

Figure 2. Block diagram of a stand alone PMU.

- V/I analog channel: the analog inputs are current and voltage signals obtained from the current and voltage transformers. In most cases, magnetic core Voltage and Current Transformers (VTs and CTs) are connected to the PMU. To minimize the phase errors introduced by instrument transformers, compensation routines are generally implemented in commercial PMUs.
- A/D converter: the Analog to Digital converter is a circuit that makes suitable the acquired signals suitable for the microprocessor. The conversion is disciplined by the time synchronization module, generally using the Phase Locked Loop control circuit (PLL). Currently, most devices on the market use sampling frequencies of the order of tens of kilosamples per second.
- Time Synchronization: this unit is able to keep the UTC time required from the standard to synchronize the measurements. There are different suitable source of synchronization: GPS is currently the most common solution for the synchronization of PMUs. A device may have an integrated GPS receiver, or may receive the synchronization signal from an external receiver. A more deeper analysis about the synchronization can be found in the section 1.2.1.
- Microprocessor: the microprocessor performs the computation necessary to estimate the quantities of interest from the acquired signals. It estimates the current and voltage phasors using the algorithms specific for the synchrophasor estimation.

Moreover, it generates the time-stamp from the synchronization module to tag the measurements. It estimates also the frequency and ROCOF.

- Data Communication: the data communication system is used to transmit the measurements from a PMU through the network, either to/from Phasor Data Concentrator, a device specially designed to receive input data from different PMUs and to make their time alignment, or to/from Monitor Station. The data communication system must be compliant with the standard for the communication of the synchrophasor IEEE C37.118.2.

1.2.1 Local time dissemination

A PMU needs the UTC time synchronization, that may be supplied directly from a GPS receiver, or from a local clock using a standard synchronization. The most common methods for the local time dissemination are:

- PPS: is a pulse train of positive pulses at a rate of one pulse per second (1 PPS). The rising edge of the pulses coincides with the seconds change in the clock and provides a very accurate time reference.
- IEEE 1588: it allows timing accuracies better than 1 μs for devices connected via a network such as Ethernet. IEEE Std C37.238-2011 specifies a subset of IEEE 1588 functionalities to be supported for power system protection, control, automation, and data communication applications utilizing an Ethernet communication architecture. A deeper description is present in paragraph 4.1.2.
- IRIG-B Standard 200-04 published by the Range Commanders Council of the U. S. Army White Sands Missile Range: the time is provided once per second in a binary coded decimal (BCD) format and an optional binary second-of-day count. The standard allows a number of configurations that are designated as Bxyz where x indicates the modulation technique, y indicates the counts included in the message, and z indicates the interval. The most commonly used form is B122, which has seconds through day-of-year coded in BCD and is amplitude modulated on a 1 kHz carrier.

1.3 The definition of synchrophasor, frequency and ROCOF

1.3.1 Synchrophasor definition

A sinusoidal signal can be defined by the following formula:

$$x(t) = X_m \cdot \cos(2\pi f t + \varphi) \tag{1.1}$$

where X_m is the amplitude and f is the frequency. Such signal is commonly represented as the complex phasor:

$$\boldsymbol{X} = \frac{X_m}{\sqrt{2}} e^{j\varphi} = \frac{X_m}{\sqrt{2}} (cos\,\varphi + j\,sin\,\varphi) = X_r + jX_i \tag{1.2}$$

where the magnitude is the root-mean-square (rms) value, $\frac{X_m}{\sqrt{2}}$, and the X_r and X_i are the real and imaginary parts of the complex value (its rectangular components). The value of phase angle φ depends on the time reference. Particularly, when t = 0 is assumed, for the standard the synchrophasor can be defined as:

The synchrophasor representation of the signal x(t) in Equation (1.1) is the value ***X*** *in Equation (1.2) where φ is the instantaneous phase angle relative to a cosine function at the nominal system frequency synchronized to UTC.*

Figure 3 shows the convention for the synchrophasor representation: the cosine functions X_{1m} has a maximum at t = 0, so the synchrophasor angle is 0 degrees when the maximum of $\mathbf{X_{1m}}$ occurs at the UTC second rollover (1 PPS time signal). Instead, the synchrophasor angle of the sine X_{2m} function is –90° degrees when the positive zero crossing occurs at the UTC second rollover.

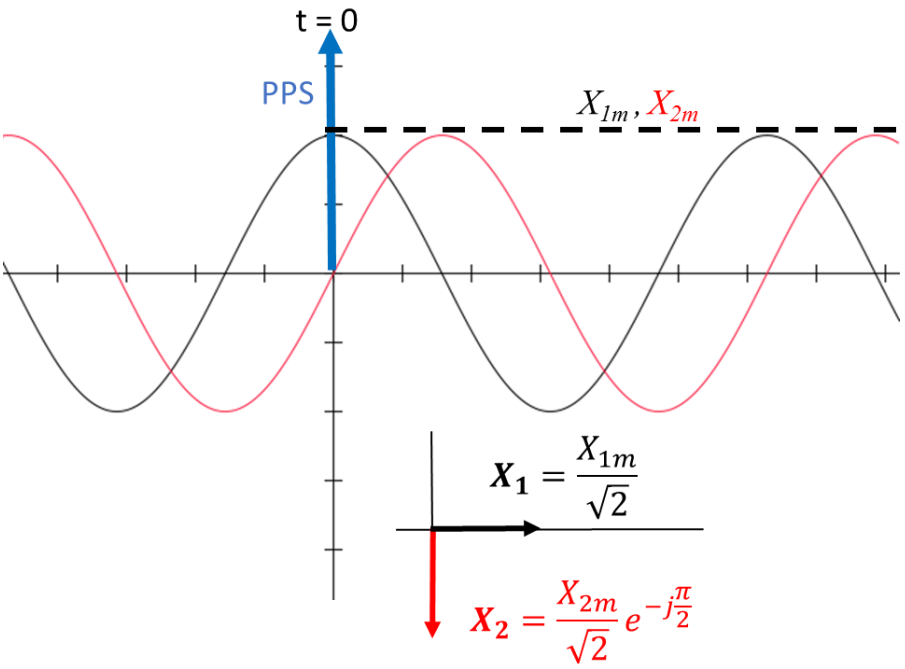

Figure 3. Convention for synchrophasor representation.

In the case where the frequency *f(t)* is a function of time, it is possible to define the function $g(t) = f(t) - f_0$ where f_0 is the nominal frequency and *g(t)* is the instantaneous frequency deviation from the nominal. The waveform representation becomes as follows:

$$\begin{aligned} x(t) &= X_m(t) \cdot \cos\left(2\pi \cdot \int f(t)dt + \varphi\right) \\ &= X_m(t) \cdot \cos\left(2\pi f_0 t + (2\pi \int g(t)dt + \varphi)\right) \end{aligned} \tag{1.3}$$

where the amplitude $X_m(t)$ is also function of time.

The dynamic synchrophasor, where magnitude and phase angle are functions of the time is represented by:

$$\boldsymbol{X(t)} = \frac{X_m(t)}{\sqrt{2}} e^{j(2\pi \int g(t)dt + \varphi)} \tag{1.4}$$

A special case where X_m is constant and $g = \Delta f = f - f_o$ is a constant offset from the nominal frequency f_0, is:

$$\boldsymbol{X(t)} = \frac{X_m}{\sqrt{2}} e^{j(2\pi \Delta f t + \varphi)} \tag{1.5}$$

where the phasor rotates at the uniform rate Δf, the difference between the actual frequency and system nominal frequency, that produces the effect in Figure 4.

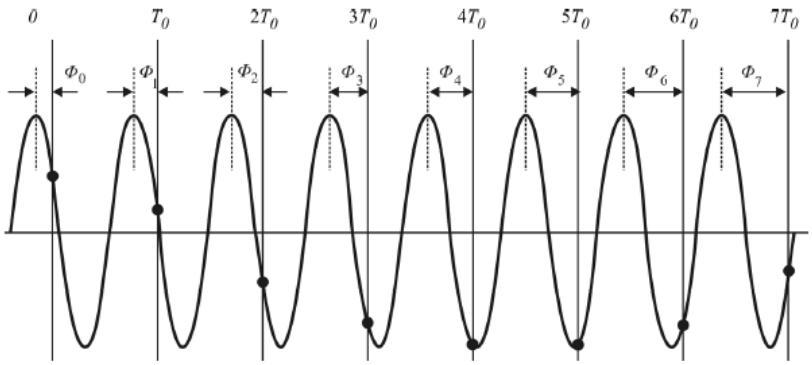

Figure 4. Sinusoid with a frequency $f>f_0$ observed at instants that are multiples of T_0.

If the sinusoid frequency f if different from f_0 but $f < 2f_0$, the phasor calculated from the waveform will have a constant magnitude, but the phase angles of the sequence of phasors calculated every T_0 will change uniformly at a rate $2\pi(f - f_0)T_0$

1.3.2 Frequency and ROCOF definitions

The standard also defines a way to measure the frequency and ROCOF, with a sinusoidal signal given by the formula:

$$x(t) = X_m \cdot \cos(\theta(t)) \tag{1.6}$$

the frequency is defined as:

$$f(t) = \frac{1}{2\pi} \cdot \frac{d\theta(t)}{dt} \tag{1.7}$$

and the ROCOF:

$$ROCOF(t) = \frac{d\left(\frac{1}{2\pi} \cdot \frac{d\theta(t)}{dt}\right)}{dt} = \frac{df(t)}{dt} \tag{1.8}$$

If the argument of the cosine in the (1.6) is represented as:

$\theta(t) = 2\pi f_0 t + \varphi(t) = 2\pi \cdot [f_0 t + \varphi(t)/2\pi]$ the formula of the frequency becomes:

$$f(t) = f_0 + \frac{d\left(\frac{\varphi(t)}{2\pi}\right)}{dt} = f_0 + \Delta f(t) \tag{1.9}$$

with $\Delta f(t)$ as the deviation from the nominal system frequency and the ROCOF becomes:

$$ROCOF(t) = \frac{d^2\left(\frac{\varphi(t)}{2\pi}\right)}{dt^2} = \frac{d\Delta f(t)}{dt} \tag{1.10}$$

1.4 Measurement evaluations

In the standard C37.118-2005 the only index to evaluate the performance of PMU was the TVE, but many works demonstrated that the aggregated information of TVE is not sufficient to completely describe measurement performance. In 2011, with the new standard, other indices are presented to evaluate the performance of synchrophasor, frequency and ROCOF measurements, under particular conditions, as in presence of step tests.

1.4.1 TVE

The TVE is an important index to evaluate the performance of synchrophasor estimation. For many years, it was the only parameter to evaluate the accuracy of a measure in steady state and dynamic conditions. The TVE is an aggregated index, which represents the vector error between the theoretical synchrophasor and the estimated one, given by the unit under test at the same instant of time. The formula of TVE is:

$$TVE(n) = \sqrt{\frac{(\hat{X}_r(n) - X_r(n))^2 + (\hat{X}_\iota(n) + X_i(n))^2}{(X_r(n))^2 + (X_i(n))^2}} \tag{1.11}$$

where $\hat{X}_r(n)$ and $\hat{X}_\iota(n)$ are the real and the imaginary parts of the estimated synchrophasor at the time instant (n).

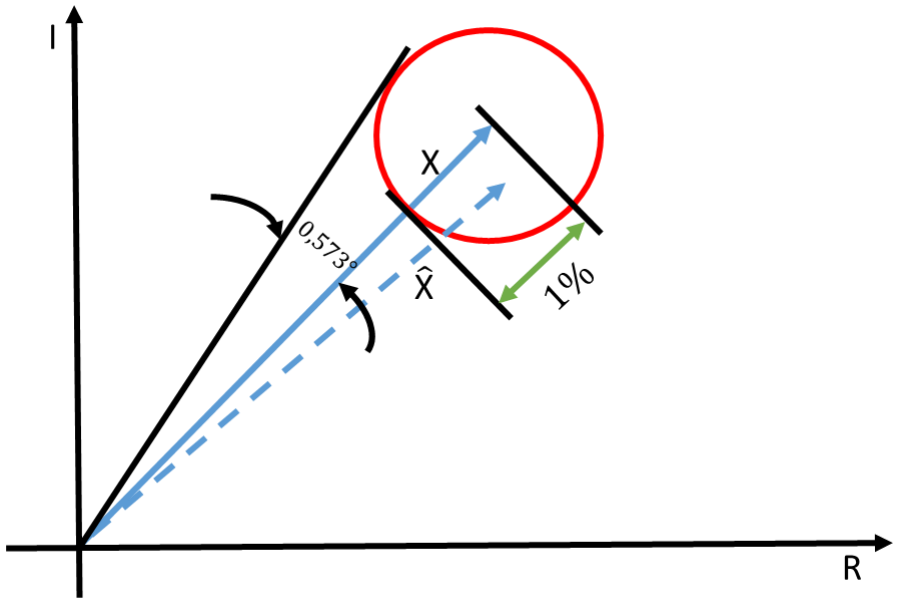

Figure 5. The TVE criterion shown on the end of phasor.

Figure 5, presents the graphical representation of the permitted TVE error (the small circle drawn on the end of the phasor). For example, when the maximum TVE error is 1 % and the magnitude error is zero, the maximum error in angle is just under 0.573º.

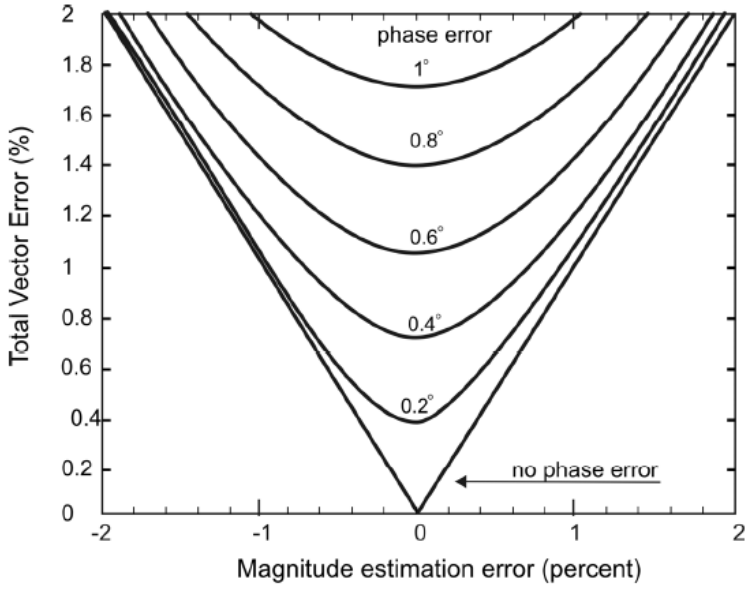

Figure 6. TVE % as a function of magnitude for various phase errors.

TVE combines magnitude and phase errors. In Figure 6 and Figure 7 there is the TVE as function of the magnitude and of the phase error respectively. The TVE is computed relative to measurement magnitude and phase at the given system frequency. Time synchronization errors will result in different TVE depending on the actual system frequency. A cycle at system frequency is 20 ms at 50 Hz and 16.67 ms at 60 Hz. One degree of phase angle at 50 Hz is 55.6 μs and at 60 Hz is 46.3 μs. Therefore the timing error that will cause a 1 % TVE error are ±31.7 μs at 50 Hz and ±26 μs at 60 Hz.

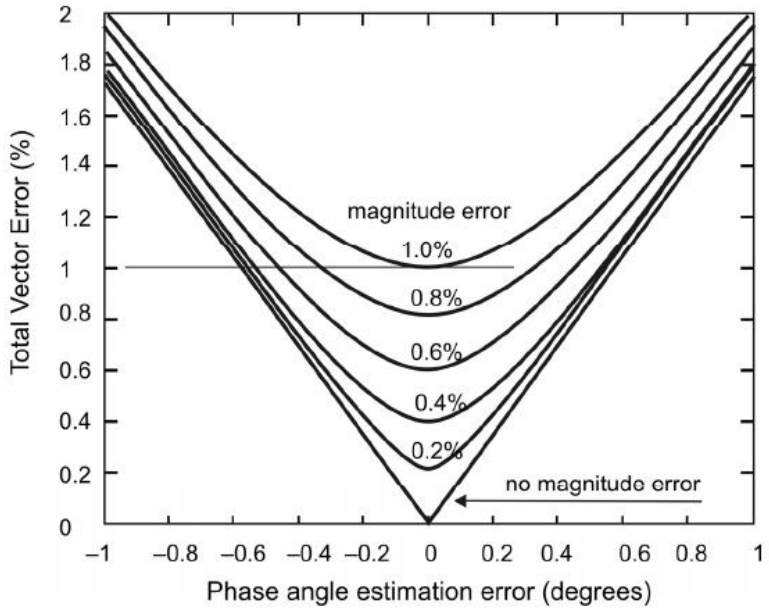

Figure 7. TVE as a function of phase for various magnitude errors.

1.4.2 Frequency Error and ROCOF error

Frequency and ROCOF are the new quantities of interest in the synchrophasor standard. The index to evaluate the accuracy of the frequency measurement is the frequency measurement error (FE) that is defined as:

$$FE = |f_{true} - f_{measured}| = |\Delta f_{true} - \Delta f_{measured}| \tag{1.12}$$

that is the absolute value of the difference between the theoretical frequency and the estimated one at the same time instant.

$$RFE = \left|\left(\frac{df}{dt}\right)_{true} - \left(\frac{df}{dt}\right)_{measured}\right| \tag{1.13}$$

The ROCOF measurement error (RFE) is the absolute value of the difference between the theoretical rate of change of frequency and the estimated one at the same time instant.

1.4.3 Indices for step tests

In the new standard three new indices are introduced to evaluate the performance in presence of step changes: the measurement response time, the delay time and the overshoot.

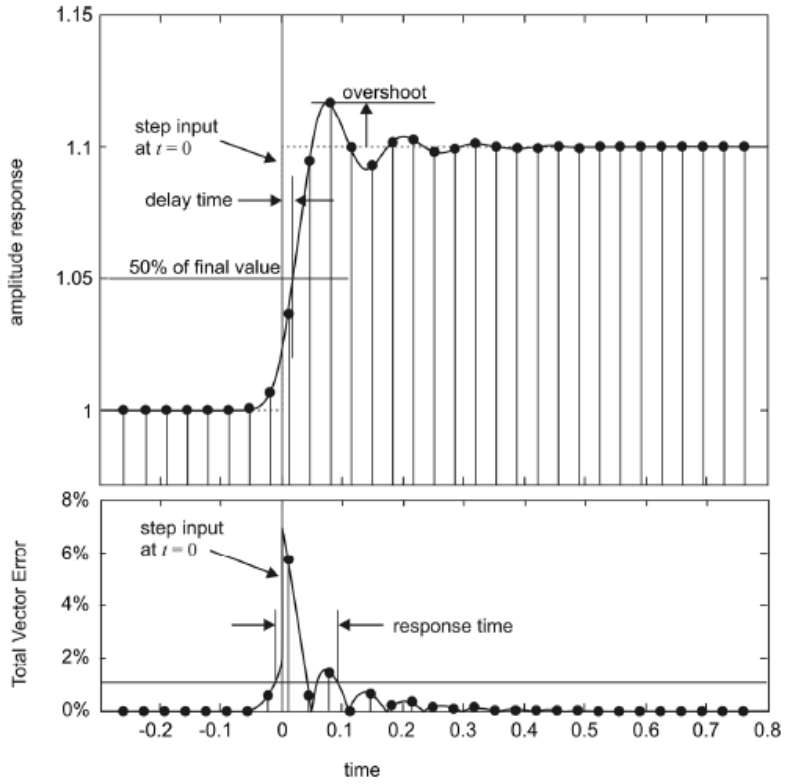

Figure 8. Example of a step change measurement with all the indices for this test. Step at t=0.

The TVE is not able to evaluate correctly the performance under step change conditions because in a fast variation it is important to evaluate the transition time between two steady-state measurements, before and after a step change is applied to the input. For the standard, the measurement response time (t_r or Δt_r) should be determined as the difference between the time that the measurement leaves a specified accuracy limit and the time it re-enters and stays within that limit when a step change, positive or negative is applied to the PMU input. This response time is important for the protection applications of the PMU and it is valid for the synchrophasor, frequency and ROCOF measurements.

The measurement delay time is another index introduced to measure the time interval between the instant when a step change is applied to the input of a PMU and the instant when

stepped measured quantity achieves a value that is halfway between the initial and final steady-state values. The purpose of evaluating the measurement delay time is to verify that the time tagging of the synchrophasor measurement has been properly compensated for the group delay.

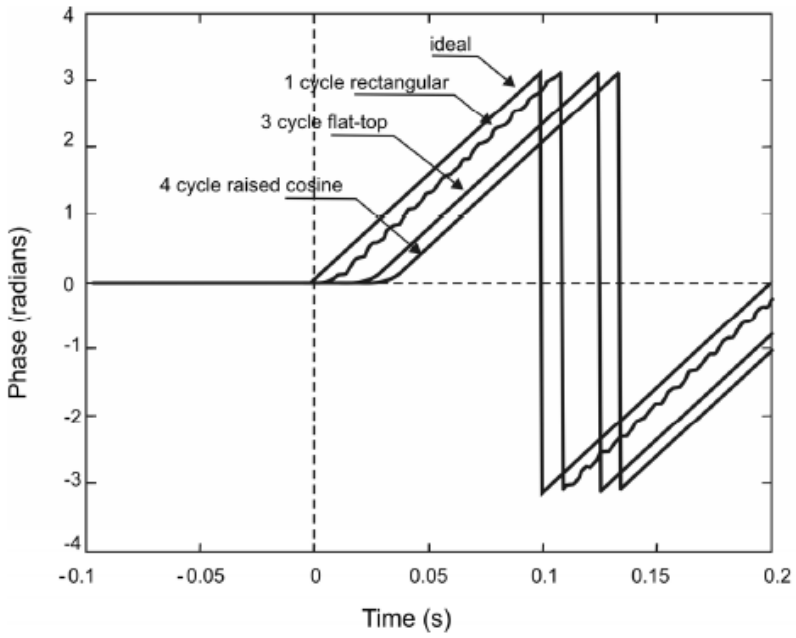

Figure 9. Frequency step test phase response without group delay compensation. Step at *t=0*.

Figure 9, from the standard, shows the effect of group delay in presence of a frequency step test without compensation.

The overshoot, as shown in Figure 8, is the maximum (or minimum for undershoot) peak value of the results curve measured from the desired response of the system. It is very important to evaluate the performance of the so-called dynamic algorithms that use the derivatives of synchrophasor for a better estimation.

1.4.4 The latency

The latency is one of the most important parameters to evaluate a PMU and is defined as the time delay from when an event occurs on the power system to the time instant when it is reported in measurement data. It can include different factors as sampling windows, PMU processing, measurement filtering, etc.

The limit given by the standard for this parameter is directly connected to the reporting rate and to of the class of performance. In Table 2 the maximum measurement reporting latency for the two performance classes is reported.

Table 2. Measurement reporting latency.

Performance class	Maximum measurement reporting latency [s]
P class	$\frac{2}{Fs}$
M class	$\frac{5}{Fs}$

1.5 Measurement compliance tests

All the compliance tests described in this subsection can be found in the synchrophasor standard but all the values are shown for reporting rate Fs higher than or equal to 25 measurements per second. In the following, the compliance requirements used to perform the tests for synchrophasor, frequency and ROCOF under steady state, dynamic and step change conditions, are shown.

1.5.1 Steady state compliance

The steady state compliance tests for synchrophasor, frequency and ROCOF are described in Table 3. Every row corresponds to a different test with a different influence quantity. The steady state compliance will be verified comparing the measurements of synchrophasor, frequency and ROCOF with the theoretical value of the same quantity, as previously described. For every tests, the maximum TVE % is equal to 1 % for both P and M class, whereas the frequency and ROCOF requirements depend on the specific test.

Table 3. Steady state synchrophasor, frequency and ROCOF measurement requirements for a reporting rate Fs ≥ 25 frames/s.

Influence quantity	Reference condition	Minimum range of influence quantity over which PMU shall be within given TVE Limits / error requirements for frequency and ROCOF compliance			
		P class		M class	
		Range	Max TVE [%]	Range	Max TVE [%]
			Max FE [Hz]		Max FE [Hz]
			Max RFE [Hz/s]		Max RFE [Hz/s]
$f_0 \pm f_{dev}$	f_0	±2	1	±5	1
			0.005		0.005
			0.01		0.01
Signal Magnitude Voltage	100% rated	80 % to 120 %	1	10 % to 120 %	1
Signal Magnitude Current	100% rated	10 % to 200 %	1	10 % to 200 %	1
Phase angle with $\lvert f_{in}-f_0 \rvert$<0.25 Hz	Constant or slowly varying angle	±π	1	±π	1
Harmonic distortion with single harmonic	<0.2 % THD	1 % each harmonic up to 50th	1	10 % each harmonic up to 50th	1
			0.005		0.025
			0.1		6
Out of band interference signal	<0.2 % of the input signal magnitude		None	10% of input signal magnitude	1.3
			None		0.01
			None		0.1

The out of band interference signal test is not required for the P class but is necessary for the compliance with the M class. This test depends on the reporting rate: Figure 10 shows the area of interest for the out of band compliance tests for a reporting rate equal to 50 frames/s. The synchrophasor standard defines the passband area of the synchrophasor measurement in a range $\pm \frac{Fs}{2}$ around f_0. An interfering signal outside the passband area is a signal with a frequency from 0 to $f_0 - \frac{Fs}{2}$ and higher than $f_0 + \frac{Fs}{2}$, but for the test the interfering signal frequency is limited up to the first harmonic ($2 \cdot f_0$). Compliance with out of band rejection can be confirmed by using a single frequency sinusoid added to the fundamental. The signal frequency of the reference signal is varied over a range $f_0 \pm 10\ \% \frac{Fs}{2}$. It is important to highlight that the frequency and ROCOF requirements in out of band test is stricter than the in harmonic tests with the same magnitude of the interfering signal.

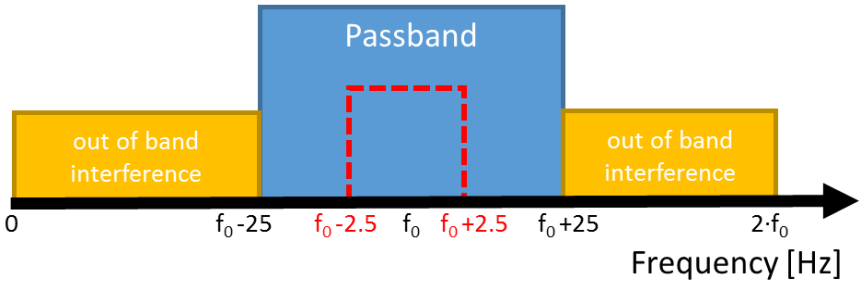

Figure 10. Out of band interference area for a reporting rate equal to 50 Fs.

1.5.2 Dynamic compliance

The dynamic compliance tests are divided in two parts: the dynamic tests for PMU bandwidth measurement and the frequency ramp test, whose limits are shown in Table 4. The measurement of the bandwidth should be determined by the variation of the input with sinusoidal amplitude and phase modulations. Mathematically, the input signals may be represented by:

$$X = X_m[1 + k_x\cos(2\pi f_{mod})] \cdot cos[2\pi f_0 + k_a\cos(2\pi f_{mod} - \pi)] \quad (1.14)$$

where X_m is the amplitude of the input signal, $f_{mod}$is the modulation frequency, f_0 is the nominal power system frequency, k_x is the amplitude modulation factor and k_a is the phase angle modulation factor. The tests for the measurement of the bandwidth are two, a case with amplitude modulation $k_x = 10$ % and a second case with amplitude and phase combined modulations. For every test, the required levels of maximum TVE, frequency and ROCOF are the same.

The frequency ramp test is performed with a linear ramp of the system frequency. The signal is given by:

$$X = X_m[\cos(2\pi f_0 t + \pi R f t^2)] \quad (1.15)$$

where Rf is the frequency ramp rate in hertz per second (Hz/s) and is the same for both P class and M class. The TVE limit for this tests is 1 % but the frequency range depends of the class of accuracy.

Table 4. Dynamic synchrophasor, frequency and ROCOF measurement requirements for a reporting rate Fs ≥ 25 frame/s.

Influence quantity	**Reference condition**	**Minimum range of influence quantity over which PMU shall be within given TVE Limits / error requirements for frequency and ROCOF compliance**			
		P class		**M class**	
		Range	**Max TVE [%]**	**Range**	**Max TVE [%]**
			Max FE [Hz]		**Max FE [Hz]**
			Max RFE [Hz/s]		**Max RFE [Hz/s]**
Modulation level: kx=0.1 ka=0.1 rad	100% rated signal magnitude $f_{nominal}$	Modulation frequency 2 Hz	3 0.06 3	Modulation frequency 5 Hz	3 0.3 30
Modulation level: kx=0 ka=0.1 rad	100% rated signal magnitude $f_{nominal}$	Modulation frequency 2 Hz	3 0.06 3	Modulation frequency 5 Hz	3 0.3 30
Linear frequency ramp	100 % rated signal magnitude and $f_{nominal}$ at start the test with ramp rate ±1 Hz /s	Ramp range ±2 Hz of $f_{nominal}$	1 0.01 0.1	Ramp range ±5 Hz of $f_{nominal}$	1 0.005 0.1

1.5.3 Step change

The step change is a particular case of dynamic condition and for clarity is treated in a dedicated section (Table 5). The test signal presents a transition between two steady states and is used to determine the specific parameters of the step responses: the response time, the delay time and the overshoot. The test signal can be determined by applying the formula in the following:

$$X = X_m[1 + \mathrm{k}_x f_1(t)]cos[2\pi f_0 t \cdot \mathrm{k}_a f_1(t)] \tag{1.16}$$

where X_m is the amplitude signal level, f_0 is the nominal power system frequency, $f_1(t)$ is the unit step function and k_x and k_a are the step size of magnitude and phase. For the protection application of the P class accuracy all the requirements are stricter than for the M class.

Table 5. Phasor, frequency and ROCOF performance requirements for input step change for reporting rate from 25 up to 50 frame/s.

Step change specification	**Reference condition**	**Maximum response time, delay time and overshoot**					
		P class			**M class**		
		Response time [s]	**Delay time [s]**	**Max overshoot or undershoot**	**Response time [s]**	**Delay time [s]**	**Max overshoot or undershoot**
		Frequency response time [s]			**Frequency response time [s]**		
		ROCOF response time [s]			**ROCOF response time [s]**		
Magnitude ± 10% kx = 0.1	All test conditions nominal at start or end of step	$1.7/f_0$	$\frac{1}{4 \cdot Fs}$	5 % of magnitude step	0.231 - 0.050		10 % of magnitude step
		$3.5/f_0$			0.328 - 0.059		
		$4/f_0$			0.369 - 0.061		
Phase ± 10° ka = ± 10°	All test conditions nominal at start or end of step	$1.7/f_0$	$\frac{1}{4 \cdot Fs}$	5 % of magnitude step	0.231 - 0.050		10 % of magnitude step
		$3.5/f_0$			0.328 - 0.059		
		$4/f_0$			0.369 - 0.061		

1.6 Other standards of interests in synchrophasor measurement

1.6.1 IEEE C37.118.2-2011

The IEEE C37.118.2 describes the way to exchange synchronized phasor measurement data between power system devices. Moreover, it specifies messaging that can be used with different communication protocols for real-time communication between PMUs, phasor data concentrators (PDCs), and other applications to control and store the measurements. It defines message types, contents, use and format for the communications.

1.6.2 IEEE C37.242-2013

The standard IEEE C37.242-2013 “Guidance for synchronization, calibration, testing, and installation of phasor measurement units (PMUs) applied in power systems” provides different aspects about PMU. The standard includes considerations for the installation of PMU devices in

electrical substations, techniques focusing on the overall accuracy and availability of the time synchronization system, test and calibration procedures for PMUs for laboratory and field applications, communications testing for connecting PMUs to other devices including Phasor Data Concentrators.

1.6.3 IEC 61850-90-5

IEC 61850-90-5 "Use of IEC 61850 to transmit synchrophasor information according to IEEE C37.118" is a part of the series of standards IEC 61850 for the design of electrical substations. The 90-5 is the part for transmitting digital state and time synchronized power measurements over wide area networks enabling implementation of wide area measurement and protection and control (WAMPAC) systems based on the IEC 61850 protocols commonly used in substation automation. The scope of the standard, not approved yet, is to harmonize the communication of the synchrophasor protocol inside the electrical substation, compliant to the standard IEC 61850, but it also provides a more secure communication between synchrophasor measurement devices and PDC.

2 Algorithms for synchrophasor estimation

This chapter focuses on the different algorithms for synchrophasor estimation. In the first part a brief introduction of different uncertainty sources of a PMU and different electrical phenomena are shown. In the second part, two different models are used to classify the algorithm: the steady state and the dynamic model. In the last part, different tests suggested by the standard of synchrophasor are used to compare the different algorithms under several different conditions.

2.1 The sources of uncertainty

The uncertainty introduced by a PMU device can be attributed to four sources:

1) transducers;
2) data acquisition system (conditioning and sampling);
3) synchronization system;
4) phasor estimation algorithm.

The first three uncertainty sources have been deeply studied in the literature. In particular, transducers introduce an uncertainty that is related to their accuracy class. In the usual practice, magnetic core voltage and current transformers (VTs and CTs) are often employed. Their accuracy is generally limited to class 0.5, according to the definition of the standards [4] and [5]. This means, at full scale, a maximum ratio error of 0.5 % and a maximum phase error of 6 mrad for VTs (9 mrad for CTs).

To minimize the effect of the ratio and phase errors introduced by instrument transformers, compensation routines are usually implemented in commercial PMUs (e.g., [6]). However, the aforementioned compensation requires the transducers to be accurately characterized, which is impractical, particularly in existing plants, and even when it is performed, it cannot be considered totally reliable, both because of the unavoidable uncertainty in the metrological characterization of the device and because the behaviour of the transducers can also be affected by actual network and environmental conditions. Therefore, significant uncertainty is expected to affect the measurement results so that the transducer can be considered as the major source of uncertainty that a PMU can be affected by.

Data acquisition system includes analog signal conditioning devices and analog-to-digital converters (ADCs). The signal conditioning stage performs the tasks of raw signal filtering, signal amplifying, or attenuating, and its uncertainty is mainly due to system noise, nonlinearities, and

gain error. As for ADCs, in commercial PMUs, 14 or 16 bit converters are usually employed. The quantization error is therefore negligible with respect to the other uncertainty sources [7].

A PMU needs to share a common time reference with the other measurement units in the distributed measurement system. Synchronization accuracy requirements are strictly related to synchrophasor measurement performances because time deviations linearly translate into phase shifts at a given frequency. Commercial PMUs either can be equipped with an internal GPS receiver or receive input time from an external clock, usually by using IRIG-B timecode. Tolerances up to ±100 ns with respect to the UTC can be obtained. However, it is possible to imagine different synchronization architectures, for instance, relying on IEEE-1588 Precision Time Protocol (PTP), to propagate the GPS time reference to other devices in the same local area network [8]. The PTP synchronization error strongly depends on the chosen infrastructure, software, and devices. For instance, a software-only implementation has demonstrated timing deviations of 10 to 100 μs (see [9]and [10]), whereas hardware-aided implementations allow to reach tolerances lower than 1 μs. The impact of synchronization on the phase error is straightforward and must be kept into account for the overall PMU performances.

On the other hand, the uncertainty due to the digital processing stage has been often considered as a marginal contribution because, in many circumstances, the other sources of uncertainty can be prevailing. However, some studies have already pointed out that, in several practical conditions, different theoretical approaches and different algorithms may lead to significant differences in the measurement result [11], [12]. For these reasons, this uncertainty source will be analyzed more deeply in the following.

In an ideal case, the power system should work in a sinusoidal steady state, characterized by a nominal frequency of either 50 or 60 Hz. In the reality, however, voltage and current signals differ from these ideal conditions, in terms of both variable fundamental frequency and distorted waveform. As for the system frequency, the system usually operates in a narrow band around the nominal frequency, but it is possible to encounter particular occasions where the real frequency of the system is far from the nominal value (up to +4 % and – 6 %, according to [21]). Just when these critical events occur, the capability of correctly measuring the synchrophasors related to the quantities of interest may be more important than ever. Moreover, load generator outputs and key operating parameters change continually, thus causing wide range disturbances, like harmonics, interharmonics, transient components, and power swings. Non-sinusoidal events in power

systems may be classified into different categories, according to the physical nature of the resulting distorting phenomena [1], [22].

1) Harmonics and interharmonics are phenomena typically produced by power electronic devices and nonlinear loads. The frequencies of the harmonics are integer multiples of the prevailing network frequency and are usually below some kilohertz. The interharmonics can be found at all frequencies that are not an integer of the fundamental [23], and since they change position, they introduce analysis and measurement difficulties related to the change of waveform periodicity [24].
2) System faults and switching operations usually produce step changes in the voltage and current waveforms and generate very high frequency components in the signal (up to 10^5 Hz).
3) Lightning and traveling waves produce very fast transients with frequencies that may be higher than 10^6 Hz.
4) Power swings are generated by the superposition of different waveforms characterized by unequal frequencies, which are caused by a lack of equilibrium between system generation and load. This can be considered a slow phenomenon (0.1–10 Hz) and can be expressed in terms of amplitude and/or phase modulation of a sinusoidal signal.

It is important to understand which of the aforementioned phenomena are of concern in phasor estimation. According to [1], all the high-frequency non-sinusoidal events, like those arising from lightning, are easily removed from the signal input of the PMU by the filtering stage.

However, phenomena generated by fault and switching operation, like the magnitude and phase step changes, which are not representative of the state of the network, can affect the synchrophasor estimation. The synchrophasors affected by this kind of phenomena should not be considered and should be flagged to avoid their use in applications. On the other hand, in [1], it has been reported that power swings must be considered as a sequence of static conditions, and as a consequence, PMUs should be able to accurately measure them. It should be highlighted that the range considered for the power swing frequencies is superimposed to a portion of the range of frequencies of interharmonics caused by different phenomena, which, according to the previous considerations, should be filtered out. As an example, Figure 11 shows the spectrum of a sinusoidal signal with frequency ω and amplitude A_1 modulated in amplitude by a sinusoidal signal with frequency $\Delta\omega$ and amplitude A_2.

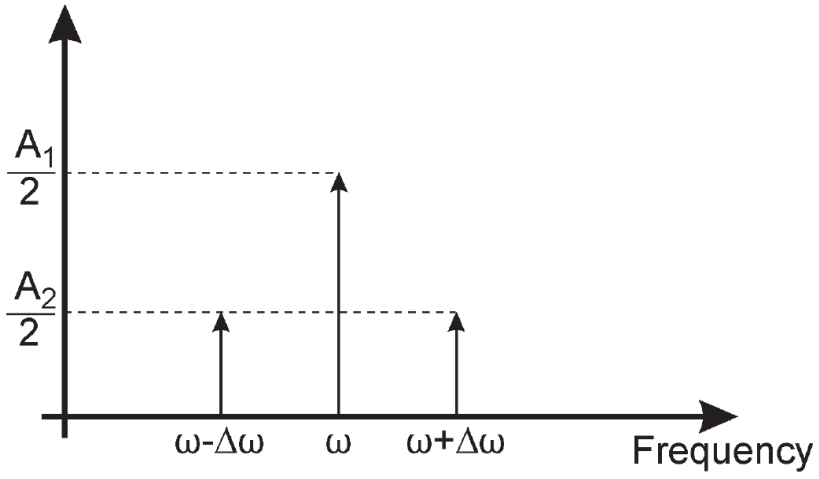

Figure 11. Spectrum of an amplitude-modulated signal.

According to [1], [25], the signal of interest is the modulating signal, which can have a frequency Δω included between 0.1 and 10 Hz. However, the spectrum of the observed signal will be included in the range [ω − Δω, ω +Δω]. This means that possible interharmonics close to the fundamental frequency of the signal could not be filtered out: in this case, the estimated synchrophasor would be incorrectly interpreted as affected by a power swing.

2.2 The synchrophasor estimation

The mathematical definition of phasor can be used to analyze power system ac signals, assuming a constant frequency. Given an ac signal *x(t)*

$$x(t) = X_m \cdot \cos(\omega t + \varphi) \tag{2.1}$$

where X_m is the signal magnitude, $\omega = 2\pi f$ is the system angular frequency, and φ is the initial phase of the signal, which depends on the definition of the time scale, its phasor representation is

$$\bar{\boldsymbol{X}} = \frac{X_m}{\sqrt{2}} e^{j\varphi} = \frac{X_m}{\sqrt{2}} \cdot \left(cos\,(\varphi) + jsen\,(\varphi)\right) = Xr + jXi \tag{2.2}$$

where *Xr* and *Xi* are real and imaginary rectangular components of the complex phasor representation. The synchrophasor estimation is based on the same concept of the phasor estimation, with the only difference that it is calculated from data samples using UTC as the time reference for the measurement.

A general representation of a power system quantity can be obtained with a modulated sinusoidal signal $x_m(t)$

$$x_m(t) = X_m g(t) \cdot \cos(\omega_0 t + \varphi(t)) \tag{2.3}$$

where $X_m g(t)$ is the modulated signal magnitude, ω_0 is the nominal system angular frequency, and $\varphi(t)$ is a real function describing phase modulation. The equivalent phasor can be defined as follows:

$$\bar{\boldsymbol{X}}(t) = a(t)\, e^{j\varphi(t)} = \frac{X_m g(t)}{\sqrt{2}} \cdot e^{j\varphi(t)} \tag{2.4}$$

The continuous time phasor definition (2.4) can be translated in the following discrete time formulation:

$$\bar{\boldsymbol{X}}(nTs) = a(nTs) e^{j\varphi(nTs)} \qquad n = 0,1,\ldots \tag{2.5}$$

where Ts is the sampling period. Definition (2.4) is well suited to follow the non-sinusoidal conditions because it highlights the time-changing behavior of phasor amplitude $a(t)$ and phase $\phi(t)$.

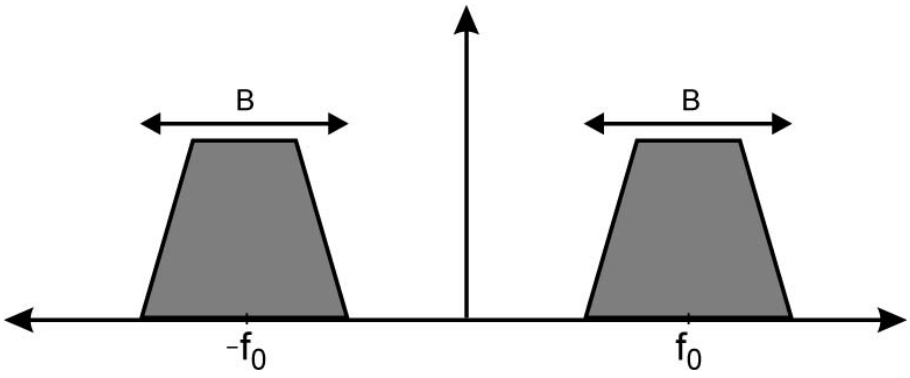

Figure 12. Qualitative behaviour of dynamic phasor model in the frequency domain.

The signal (2.3) acts like a passband signal centered at frequency f_0 (Figure 12) in the frequency domain: all the frequency components inside the band are considered meaningful, whereas the components outside the band are considered as disturbances. This model gives the dynamic reference for any synchrophasor estimation algorithm, leaving to the estimator the definition of a suitable computational procedure that allows to calculate phasors with given accuracy constraints.

2.2.1 The general model

Several algorithms have been presented in the literature to estimate phasors [2], [3],

[13-20], [25], [27], [29], [33]. Every algorithm requires a phasor model and uses specific techniques to match the model parameters. In particular, the algorithms can be divided into two main classes with respect to the measurement model: algorithms relying on a steady state phasor model and algorithms based on an intrinsically dynamic phasor model.

A general phasor model, which can be used as a common framework for both classes, describes the phasor in a specific time interval by means of a complex Taylor expansion

$$\bar{\boldsymbol{X}}_{\boldsymbol{Tr}}(\Delta t) = \sum_{k=0}^{K} \frac{a^{(k)}}{k!} \Delta t^k \, e^{j \sum_{h=0}^{k} \frac{\varphi^{(h)}}{h!} \Delta t^h} = \sum_{k=0}^{K} \frac{\bar{\boldsymbol{X}}^{(k)}}{k!} \Delta t^k \tag{2.5}$$

where $\Delta t = nTs - Tr$ is the time shift with respect to the reference time Tr, K is the Taylor expansion order, and $a^{(k)}$, $\phi^{(k)}$, and $\boldsymbol{X}^{(k)}$ are the kth derivatives at the time reference (a subscript Tr is dropped in the equations for the sake of clearness) of the phasor amplitude, angle, and complex representation, respectively. In such a model, the synchrophasor at time reference Tr is given by $\boldsymbol{X}^{(0)}$.

2.3 The steady state algorithms

The steady state phasor model can be obtained by the general formulation (2.5) considering the expansion of order $K = 0$ and is the underlying model for a wide class of algorithms. The simplest and most widespread algorithm calculates the phasor by a DFT computation applied to a given observation window (also called method **A** in the following sections)

$$\tilde{\boldsymbol{X}}_{Tr} = \frac{\sqrt{2}}{N} \sum_{n=-\frac{N}{2}}^{\frac{N}{2}-1} x(nT_s - T_r) e^{-j2\pi \frac{n}{N}} \tag{2.6}$$

where $\tilde{\boldsymbol{X}}$ is the estimated phasor and N is the number of samples in a chosen window. The DFT-based algorithm works correctly when, in stationary conditions, the observation window perfectly matches an integer number of cycle durations of the periodic signal $x(t)$. Thus, N is usually chosen as a multiple of $N_0 = 1/(f_0 \cdot T_s)$, which is the number of samples in one cycle at nominal frequency. When this condition is not met, particularly under off-nominal frequency conditions, good results can be achieved by weighting the samples with a specific window, such as Hamming or Hann (algorithm $\mathbf{A_w}$ in the following). There are algorithms that, while keeping the simple steady state model, try to compensate the errors of algorithm **A** due to dynamic

behaviour in the acquired signal. One method (here referred to as algorithm **B**) has been proposed in [1] to attenuate the effect of "negative frequency" infiltration that arises under off-nominal frequency conditions and filter the fast transient events, caused by switching operations and faults. The method is based on a three-point-filter technique and uses three partially overlapping observation windows. Each synchrophasor is obtained by calculating the DFT on a one-cycle observation window centered on the reference time and averaging it with two adjacent DFT phasors chosen such that their relative phase angles with respect to the central one are ±60° at the nominal fundamental frequency.

2.4 The dynamic algorithms

Under dynamic conditions, the static model (2.2) is not able to follow phasor changes that take place in the observation window, thus leading to an incorrect synchrophasor evaluation. The importance of following phasor dynamics has been pointed out in the literature, for instance, in [27] and [28], but the idea of considering a dynamic model to better estimate phasors has been emerging in the last years (see [3]). Algorithms based on an intrinsically dynamic model are designed to estimate the parameters (phasor derivatives) of (2.5) when the Taylor order is greater than zero. The model order is chosen as a trade-off between accuracy and computational burden.

There are algorithms that are conceived as a postprocessing step of DFT calculation aimed at correcting DFT estimation errors due to the mismatch between a dynamic model (K > 0) and the steady-state one (K = 0)[2],[13-17],[27]. In [2], for instance, the timechanging phasor is described by a first-order complex polynomial (always centered in Tr) for a four-parameter algorithm or by a second-order one for a six-parameter algorithm (referred to as method **C** in the following). The expanded model implies that, in the second-order modelling, the boxcar one-cycle DFT phasor $\widetilde{\boldsymbol{Y}}$ calculated on a window centered on *Tr* is tied to the zero-, first-, and second-order theoretical parameters. The "true" phasor $\bar{\boldsymbol{X}}^{(0)}$ is then estimated from the "correction" formula:

$$\bar{\boldsymbol{X}}^{(0)} = \widetilde{\boldsymbol{Y}} - j\frac{\bar{\boldsymbol{X}}^{(1)^*}}{2Nf_0 \sin\left(\frac{2\pi}{N}\right)} - \frac{\bar{\boldsymbol{X}}^{(1)^*}}{f_0^2}\left(\frac{N-1}{24N}\right) - \frac{\bar{\boldsymbol{X}}^{(2)^*}}{f_0^2}\frac{cos\left(\frac{2\pi}{N}\right)}{2N^2\left(sin\frac{2\pi}{N}\right)^2}24N \qquad (2.7)$$

where $\bar{\boldsymbol{X}}^{(1)^*}$ and $\bar{\boldsymbol{X}}^{(2)^*}$ are the conjugate of the first- and second-order phasor derivatives $\bar{\boldsymbol{X}}^{(1)}$ and $\bar{\boldsymbol{X}}^{(2)}$. Derivatives are computed via finite-difference formulations. For instance, $\bar{\boldsymbol{X}}^{(1)}$ can be calculated by

$$\frac{\bar{\boldsymbol{X}}^{(M)}}{f_0} \approx \frac{3}{2}\,\tilde{Y}_M - 2\tilde{Y}_{M-1} + \frac{1}{2}\,\tilde{Y}_{M-2} \tag{2.8}$$

where M is the current window index and the adjacent observation windows ($M-1$ and $M-2$) are also needed. It is interesting to note that a model of greater order requires more adjacent windows to be estimated and, as a consequence, a greater computational cost. Another technique based on the same concept can be found, for instance, in [27], where a second-order model is used and the finite-difference equations are replaced by a least squares (LS) approach. A different approach for signal analysis under oscillations is introduced in [3]. It is based on a linear filter bank that performs an LS approximation of an observation window (that can also include a noninteger number of cycles) with respect to the second-order Taylor model [$K = 2$ in (2.5)]. Unlike the algorithm introduced in [2] and [27], such algorithm directly acts on the samples, without any DFT computation. As a consequence, an arbitrary number of samples can be used, and the observation window is not required to include an integer number of cycles. A weighted LS can also be used, if different weights are given to different samples, as in [29]. The linear non-orthogonal transform, involved in the algorithm, is defined as a Taylor–Fourier transform (TFT) and is intended to approximate the bandpass signal represented by the dynamic phasor. The algorithm gives a simultaneous estimation of all the second-order model parameters, which are phasor, phasor speed, and phasor acceleration (phasor derivatives of zeroth, first, and second orders, respectively). From these parameters, it is straightforward to obtain the amplitude along with its derivatives and the phase along with the frequency and rate of change of frequency (ROCOF). The algorithm will be referred to as **method D** and due to the importance of this algorithm in the following, a deeper description of the method D or TFT-WLS is in the next paragraph is shown.

2.4.1 The algorithm TFT-WLS

In [3] and [29], a phasor estimation algorithm that applies a WLS approximation of the phasor in a given observation window based on a K-th order Taylor model has been introduced. Thus, the algorithm relies on the TFT-WLS to better follow phasor. A general model for the dynamic phasor $\boldsymbol{p}$ for $k > 0$ is in (2.5).

Given a N samples observation window, the dynamic phasor model can be translated in the following vectorial form:

$$\mathbf{s} = \mathbf{B} \cdot \mathbf{p} \tag{2.9}$$

where s is the vector of signal samples and

$$\mathbf{p} = \frac{1}{2}\left[p^{(k)}\frac{Ts^k}{k!}\cdots p^{(0)}\ p^{-(0)}\ \cdots p^{-(k)}\frac{Ts^k}{k!}\right]^T \tag{2.10}$$

and the matrix B can be expressed by its generic element:

$$b_{h,k} = \left(h - \frac{N}{2}\right)^{|K-k|} e^{(-1)^{1+\left(\frac{k}{K}\right)}j2\pi(h-\left[\frac{N}{2}\right])\frac{f_0}{T_s}} \tag{2.11}$$

for $h = 0, \ldots, N-1$ and $k = 0, \ldots, 2K$. To obtain an evaluation of **p** vector a WLS method is used, that is:

$$\hat{\mathbf{p}} = (\boldsymbol{B^H W^H W B})^{-1}\boldsymbol{B W^H W s} \tag{2.12}$$

where **W** is the weighting matrix:

$$\mathbf{W} = \begin{pmatrix} w_{11} & 0 & \ldots & 0 \\ 0 & w_{22} & \ldots & 0 \\ \vdots & \vdots & \ddots & 0 \\ 0 & 0 & 0 & w_{nn} \end{pmatrix} \tag{2.13}$$

The weights are obtained from the Kaiser windows how it is suggested in [29].

2.5 The test cases for the comparison of the different algorithms

The test cases can be divided into two main classes with respect to the dynamics of the reference signal: steady-state and dynamic conditions. Steady state includes both the ideal sinusoidal quantities and other important non-sinusoidal conditions that can be found in the practice: additive noise, amplitude and phase modulations, and presence of harmonics and interharmonics. In this class, signals that show stable characteristics over time have been included. However, it is important to underline that they can correspond both to static and dynamic phasor behaviours. On the other hand, step signals and linear frequency ramp signals have been chosen as representative of transient conditions of a power network.

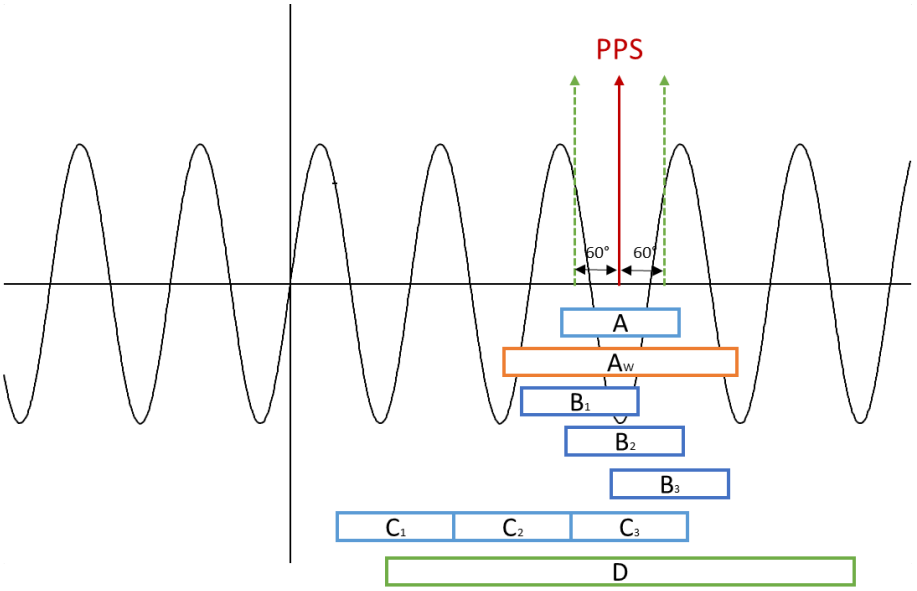

Figure 13. The number of cycles used from each algorithms.

In Figure 13 all the methods are represented. Method **A** uses a number of samples corresponding to one cycle at nominal frequency. The other algorithms employ a different number of cycles: Method **Aw** has two cycles, method **B** has three partially overlapping cycles, method **C** has three cycles, according to [2], and method **D** has four cycles, as suggested in [29]. As already mentioned, the length of the observation window and the choice of the reference time affect the delay of the synchrophasor computation.

Tests have been performed by simulations, adopting a 10-kSample/s sampling frequency. A "per sample approach" has been used, which is a phasor computation performed at every sampling period by continuously shifting the observation window by a single sample. The subsequent analyzed windows are thus overlapping, except for a sample. Each synchrophasor is referred to the reference time corresponding to the center of the estimation window. The aim is to precisely follow phasor evolution, to better test estimation algorithm behavior. In the practice, every PMU will have a tunable reporting rate ([26] suggests 10, 25, and 50 synchrophasors per second for 50-Hz power systems and 10, 12, 15, 20, 30, and 60 synchrophasors per second for 60-Hz power systems), but this is only related to real-time computational issues or bandwidth requirements for data transmission. For the methodological analysis it is better to have the fastest measurement rate so that the limit condition is investigated.

2.5.1 Steady-state tests

Noise: the tests are aimed at emphasizing the rejection property of algorithms with respect to additive white Gaussian noise.

Off nominal: represent a typical scenario in an electrical systems when the frequency is different from the nominal 50 Hz or 60 Hz.

Harmonics and **interharmonics**: harmonics and interharmonics cause signal distortion, that has to be cancelled by phasor estimation algorithm in order to retain the fundamental frequency model. As for the harmonics, in order to consider a general situation, rather than introducing one harmonic component at a time, here a signal spectrum composed by the individual harmonics indicated in the power quality standard [24] is used.

Each interharmonic can be considered as a single frequency components that is superimposed to the useful signal. Interharmonics can be extremely difficult to detect and isolate if they are located in the band of interest of the phasor dynamic model (2.4).

2.5.2 Dynamic tests

Modulation: a modulated signal can be useful to describe power swings. In [1] and [26] it is suggested to employ sinusoidal functions, at a given frequency and amplitude, to modulate the signal amplitude and phase. An amplitude modulated signal results in three spectral lines, as can be seen in Figure 11. It is clear that the modulating frequency determines the position of the two side lines and gives the bandwidth of the signal. According to [1], if the modulating frequency is above 10 Hz, the signal dynamics should be excluded from the dynamic phasor model and should be filtered out by the estimation algorithm. Amplitude and phase modulations can also be simulated separately with a modulating frequency that can vary from a few hertz up to 10 hertz.

Ramp tests: in the frequency ramp tests the reference signal undergoes a linear change of frequency at a constant rate of change (ROCOF) of 1 Hz/s for 10 s. The ramp evolves between two steady state conditions. The values of TVE in the proximity of the transitions occurring at the starting and final points of the ramp are almost meaningless and this should be kept into account, by excluding them from the analysis.

Step tests: the step tests are present in the standard to ensure the interoperability of PMUs. The tests are divided in amplitude and phase steps. Parameters to realize this type of test is suggested for instance in [25]. It is important to notice that the TVE can be a useless index in the sharp transition between two steady states, where it results in very high values in a short time period. A suitable index for this type of tests is the response time, to evaluate the promptness of the algorithms.

2.6 The tests system

To realize the tests and to study the characteristic of the algorithms proposed in this chapter a LabVIEW software is used. The main software is composed by three different parts:

- The signals generator
- The platform for the algorithms
- The results aggregator

The signal generator VI is a software able to realize all the waveform suggested in the standard C37.118.1 and to combine different dynamic and steady events to study in more grave case the performance of the algorithms. The signal generator also provides the true synchrophasor, frequency and ROCOF, essential information to calculate the TVE and other parameters to evaluate the performance.

The platform for the algorithms is able to check different and heterogeneous methods in the same time in the same tests conditions. All the algorithms need to receive the same waveforms, but in most cases, the algorithms use different number of samples, dependently of their configurations. To correlate the different number of samples for each algorithms a common reference, in the centre of the waveform, is used for every test.

The results aggregator VI implements all the indices present in the synchrophasor standard to check the performance of the algorithms. Further indices are evaluated to verify the percentage of the error of magnitude and phase that contribute to the TVE %.

2.7 The test results

2.7.1 Noise

Tests have been performed to compare all the considered algorithms when Additive White Gaussian Noise (AWGN) is added to the clean sinusoidal signal, at different levels of Signal to Noise Ratio (SNR). The limit of 1 % of TVE is respected by all the methods, for SNR above 26 dB. With a noise of 40 dB, which is often considered as a possible lower limit in actual situations, for instance, the TVEs are in the average below 0.1 %, with peaks of about 0.2 % (see also [12]).

2.7.2 Off-nominal frequencies

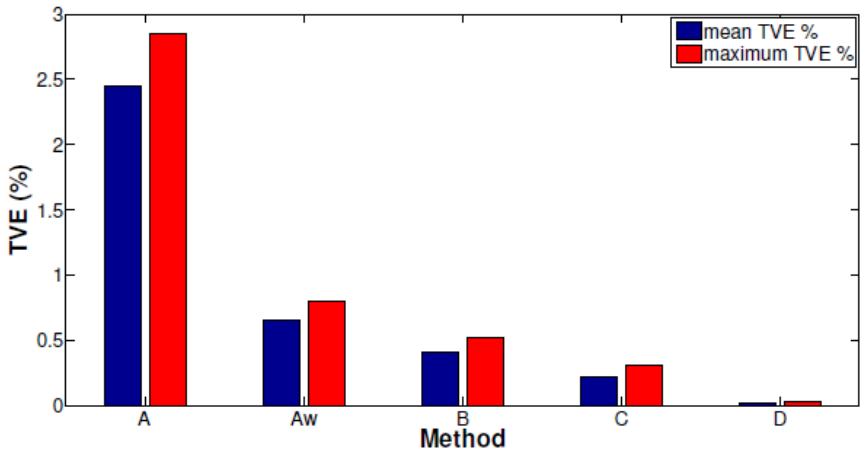

Figure 14. TVE % results for off-nominal frequency f=52.5 Hz.

In Figure 14 is shown one case for off-nominal test set; the TVE results with working frequency f = 52.5 Hz are given as example. It is shown that algorithms that rely on a dynamic phasor model have better performances even under off-nominal frequency conditions. This fact is due to the passband characteristics of such algorithms that are designed to filter disturbances and to let unaffected a signal like that of Figure 14: thus, if a sinusoidal signal oscillates at off-nominal frequency, but it is still inside the band of interest, its features are completely extracted by such algorithms.

2.7.3 Harmonics

Tests in presence of harmonics have been performed using different values for the fundamental frequency of the signal (50, 50.05, 50.5, 52.5 and 55 Hz). It should be recalled that the harmonic frequencies are multiples of the actual signal frequency. Forty harmonics were simultaneously added to the signal, with the individual harmonic levels indicated in [30] and a Total Harmonic Distortion (THD) equal to 10 %. In this case, of the test with fundamental frequency equal to 55 Hz (see Table 6). In this condition, in fact, the maximum TVE % for

methods B and C is similar: 2.52 % and 2.46 %, respectively. In some cases, then, it could be convenient to divide the two components and analyze them as separate indices to emphasize certain results, In particular, the percent amplitude error and the phase error expressed in centiradians can be compared directly with TVE % results.

In the case of algorithm B most of the TVE is caused by an amplitude error (2.48 %), whereas only a small part of it is caused by the phase error (0.84 crad). Contrariwise, algorithm C shows a phase error (2.27 crad) much larger than the amplitude error (1.61 %) pointing out a completely different behaviour.

Table 6. Maximum TVE % results for 55 Hz Harmonic Test.

Algorithms	Max TVE %
Method A	6.53
Method Aw	2.89
Method B	2.52
Method C	2.46
Method D	0.33

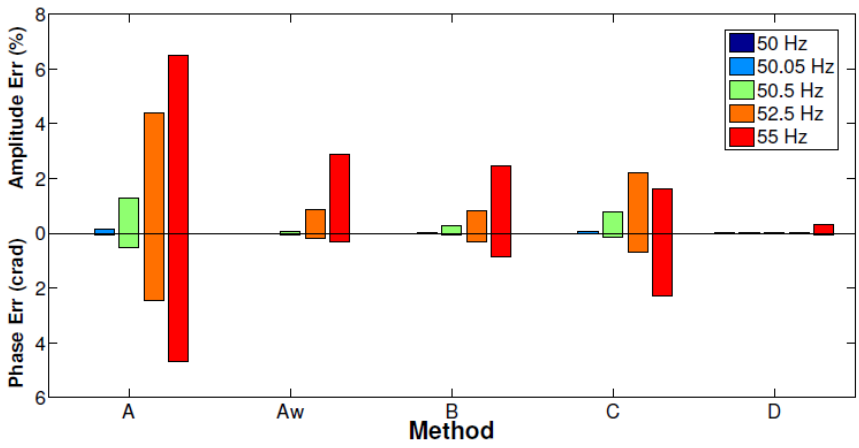

Figure 15. Maximum amplitude error (%) and phase error (crad) for the tests in presence of harmonics for different frequencies.

Figure 15 shows the results of the maximum amplitude error (%) and maximum phase error (crad) for the tests in the presence of harmonics. It can be seen that for the test at 50 Hz all the methods show a good harmonic rejection whereas for the test with fundamental frequency equal to 55 Hz, only method D presents a good harmonic rejection. It is interesting to highlight

that, while the performances at off-nominal frequencies strictly depend on the pass-band of the estimators, the harmonic rejection ability is due to the stop band characteristics. Method D, for instance, has a very flat response in the band of interest and thus, as can be seen in Figure 15, has a behaviour, in presence of harmonics, that does not depend in a significant manner on the fundamental frequency. On the contrary, method A, which perfectly cancels the effects of harmonics at nominal frequency, mainly suffers in the presence of off-nominal conditions.

2.7.4 Interharmonics

A single interharmonic line, with a 5 % amplitude with respect to the signal amplitude, has been added to a pure sinusoidal signal at nominal frequency. The interharmonic frequency f_I has been changed during tests, by a 1 Hz step, to sweep a spectrum range from 25 Hz to 95 Hz. Figure 16 shows the results for two specific interharmonics at frequencies fI = 55 Hz and 85 Hz, respectively.

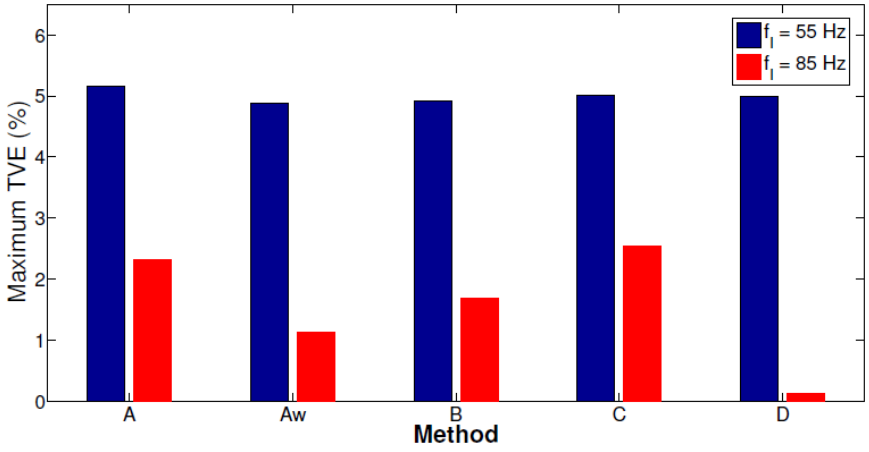

Figure 16. Maximum TVE % in presence of a single interharmonic at frequency f_i.

The behaviour of the algorithms is related to their filtering capabilities. In fact, when the interharmonic is in the pass-band of the algorithm (designed to include dynamic phenomena of interest), no rejection is obtained and thus the TVE is about 5 %, whereas, for interharmonics at higher frequencies TVE depends on the stop-band attenuation. The results are, qualitatively, the same for amplitude and phase error, because the TVE is alternatively due to the each of the two error components.

2.7.5 Modulation

In the following, results for sinusoidal modulation are reported in Table 7 and Table 8.

Table 7. Maximum amplitude and phase error for amplitude modulated signal (kx=0.1 and fm = 5Hz).

Algorithms	50 Hz		51 Hz	
	Max Amplitude Error (%)	**Max Phase Error (crad)**	**Max Amplitude Error (%)**	**Max Phase Error (crad)**
Method A	0.55	0.50	1.21	1.20
Method Aw	0.29	0.03	0.39	0.17
Method B	0.25	0.03	0.28	0.11
Method C	0.18	0.07	0.23	0.15
Method D	0.03	0.01	0.04	0.03

Table 7 shows the maximum percent amplitude error and maximum phase error for two different system frequencies, when an amplitude modulated signal is used (k_x = 0.1 and f_m = 5 Hz). Algorithms designed on a dynamic model outperform the others under phasor amplitude variations. It can also be highlighted that the behaviour is related to the off-nominal characteristics: in fact, if the estimation method is based on a pass-band model, it gives good results when the system frequency is off-nominal. If the test signal is also modulated in phase, by a sinusoidal modulating function, the band of the signal can be computed by means of a Fourier series that involves Bessel functions of first kind (see [31] for details). For k_a = 1, the spectrum can be limited to ± 2 f_m with respect to the fundamental frequency. In Table 8, results of tests performed with simultaneous amplitude and phase modulations for two different frequencies are given. Similarly to the previous test, method D is able to follow amplitude and phase variations.

Table 8. Maximum amplitude and phase error for amplitude and phase modulated signal (kx,ka = 0.1 and fm = 5 Hz).

Algorithms	50 Hz		51 Hz	
	Max Amplitude Error (%)	**Max Phase Error (crad)**	**Max Amplitude Error (%)**	**Max Phase Error (crad)**
Method A	0.74	0.77	1.69	1.71
Method Aw	0.29	0.27	0.44	0.38
Method B	0.27	0.24	0.30	0.28
Method C	0.22	0.22	0.28	0.31
Method D	0.04	0.04	0.06	0.06

2.7.6 Ramp tests

Several frequency ramp tests have been executed choosing different ROCOF varying from ± 0.01 Hz/s to ± 1 Hz/s.

Table 9. Maximum module and phase results for ramp test for ramp test with ROCOF = 1 Hz/s.

Algorithms	Max Amplitude Error (%)	Max Phase Error (crad)
Method A	6.71	3.05
Method Aw	2.85	0.23
Method B	2.22	0.38
Method C	0.98	1.43
Method D	0.32	0.23

Table 9. shows the results of the maximum amplitude error (%) and maximum phase error (crad) of the ramp test with a ROCOF of 1 Hz/s. Also in this case, methods based on a dynamic model perform better then methods based on a static model. This is due to their off-nominal frequency behaviour and tracking capabilities.

2.7.7 Step tests

In order to study the impact of faults and switching operations on the synchrophasor estimation, several tests with amplitude and phase steps have been executed. During the simulations, the signal instantaneously passes from a steady-state condition to another steady-state condition. To analyse the dynamic behaviour of the studied methods, the TVE response time with two different threshold levels (*Ht = 1 %* and *Ht = 3 %*)

1) Amplitude Step: the original signal is a 50 Hz sinusoidal waveform. Two step conditions have been considered during which the amplitude of the observed signal is instantaneously reduced by 20 % and the 50 %, respectively.

2) Phase Step: the initial steady state condition is again characterized by a frequency of 50 Hz. Two tests have been performed, where the phase instantaneously passes from 0° to +15° and +45° respectively.

It should be highlighted that the T_r may be misleading because it is strictly dependent on the chosen threshold *Ht*. As an example, Figure 17 shows the TVE trends of the five methods for the -20 % magnitude step test. Threshold *Ht* = 1 % and *Ht*= 3 % have been indicated in Figure 17 with two dashed horizontal lines. It is possible to see that, if 3 % is considered as threshold, all the methods presents similar TVE response time. These may be interpretable as a similar behaviour of both the algorithms designed on a static and dynamic model. However, if 1 % is chosen as threshold, algorithms C and D show a completely different behaviour characterized by a T_r much bigger than methods A and B. t_R values for *Ht* = 1 % and *Ht* = 3 % have been reported in Table 10.

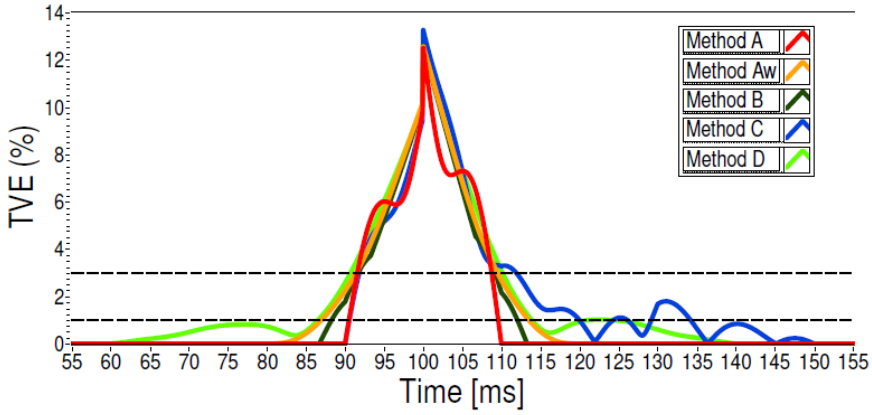

Figure 17. TVE trends for the -20 % magnitude step test.

Table 10. Δt_r values for Ht = 1 % and Ht = 3 % in the -20 % amplitude step test.

Algorithms	Δtr (ms)	
	Ht = 1 %	**Ht = 3 %**
Method A	19	17
Method Aw	27	18
Method B	24	18
Method C	44	20
Method D	38	20

2.7.8 Final considerations

Table 11. Summary of method performances.

	Static phasor model			Dynamic phasor model	
Test conditions	**Method A**	**Method Aw**	**Method B**	**Method C**	**Method D**
Off-nominal	LOW	MEDIUM	MEDIUM	HIGH	HIGH
Harmonics	LOW	MEDIUM	MEDIUM	LOW	HIGH
Modulation	LOW	MEDIUM	MEDIUM	MEDIUM	HIGH
Ramp	LOW	MEDIUM	MEDIUM	MEDIUM	HIGH
Step	HIGH	MEDIUM	MEDIUM	LOW	LOW

In Table 11, a summary of analyzed method performances is reported. The quality of each method with respect to a single aspect or test condition is expressed by means of a three-level (LOW,MEDIUM, and HIGH) qualitative scale. From the table, it is possible to see that the methods based on a dynamic model perform better under off-nominal conditions or oscillations.

Nevertheless, method C is prone to the presence of harmonics in off-nominal conditions. It can also be noticed that methods that rely on a longer observation window have usually slow response times. It should be underlined that the computational burden increases with the algorithm complexity (from A to D).

3 Proposals to improve the performance in the synchrophasor estimation

This chapter is divided in two parts, each one describing a different evolution of the idea to improve the performance of the dynamic algorithm called method D (or TFT-WLS) discussed in Chapter 2. The good performance shown in the tests, but with some lacks in dynamic, cases suggested to use this algorithm, with suitable modifications, to match all the criteria indicated by the synchrophasor standard.

The idea behind each proposal is to improve the performance of the TFT-WLS to realize an algorithm with good performance for the protection class and, in the same time, good accuracy in terms of measurement.

At the end of every proposal different tests are shown to verify the compliance of the algorithm.

3.1 Fast response to changing conditions

In the previous chapter, several algorithms under steady state and dynamic conditions have been reported. The classical approach to synchrophasor measurement consists of a Discrete Fourier Transform (DFT) applied over an observation window centred on the synchrophasor reference instant. Under dynamic conditions, the DFT based algorithm is not able to follow phasor changes that take place inside the observation window, thus leading to an incorrect synchrophasor evaluation. Better results can be achieved by combining the DFT with specific weighting windows, such as Hamming or Hann.

Besides, there is a class of algorithms that are conceived as a post-processing step of DFT calculation aimed at correcting DFT estimation errors due to non-stationary conditions. Methods proposed in [32], [33] consider the phasor as a Taylor expansion around the estimation point and estimate the synchrophasor through compensation of the errors introduced in DFT computation by the mismatch with the stationary model.

In the chapter 2 the behaviour of the TFT-WLS algorithms under different stationary and non-stationary conditions has been analysed by using different performance indices (e.g. TVE, response time, magnitude and phase error). According to the results (see the Table 11), the method D, called in the following TFT-WLS, outperforms the others in all the conditions except under step tests, where the TFT-WLS algorithm has shown some room for improvement.

In the next subsection, a modified version of the TFT-WLS algorithm is presented with the aim to improve its behaviour during transient conditions. In particular, an adaptive algorithm

is proposed, that allows to understand when the signal is undergoing fast changes and, then, to refine phasor estimation.

3.1.1 Proposed algorithm modification

The phasor estimation algorithm TFT-WLS is based on a fixed number of samples and a fixed weighting window. To obtain a faster response to abrupt phasor dynamic changes, like amplitude or phase steps, an adaptive approach is proposed here. The underlying idea is to detect degradation in the TFT estimation, due to a mismatch between the signal and the chosen model, and to adapt the estimation algorithm to changing conditions.

The modified algorithm follows three main steps:

1. Calculation of standard phasor.
2. Evaluation of the estimation error and detection of critical conditions.
3. Computation of adapted estimation.

After the TFT computation of the phasor, a procedure of error evaluation is needed to start any adaptation algorithm to refine the estimation. An index relying on the signal reconstruction has been chosen to detect the quality of phasor estimation. In particular, the following Error Monitor function has been used, inspired by the transient monitor in [1]:

$$\mathbf{EM} \triangleq \sum_{k=0}^{N-1} \frac{|s(k) - \tilde{s}(k)|^2}{N} \tag{3.1}$$

where N is the number of samples in the observation window and $\tilde{s}(k)$ is the signal reconstructed from the estimated phasor parameters. $\tilde{s}(k)$ is obtained by using the estimated phasor parameters in (3.2):

$$\hat{\mathbf{s}} = \mathbf{B} \cdot \hat{\mathbf{p}} \tag{3.2}$$

The EM function represents the average error energy in signal reconstruction and thus allows understanding when the signal is not perfectly described by the Taylor series parameters given by (2.12) in the whole observation window. If the EM overcomes a given threshold, an observation window can be labelled as critical and the adaptive algorithm is started. In some cases, for instance in presence of harmonics, such criterion can be too soft and may not be perfectly tuned to detect only transient conditions. Then, other criteria can be added, such as an evaluation of the degree of unbalance of the energy of the reconstruction error along the

observation window. For instance, in the tests of the following section, a combined criterion has been used:

$$\left(\frac{EM}{a^2} > \alpha_{th}\right) \wedge \left(\frac{|EM_1 - EM_2|}{a^2} > \beta_{th}\right) \rightarrow \ critical\ condition \tag{3.3}$$

where $a=|p^{(0)}|$ is the amplitude of the estimated phasor, α_{th} and β_{th} are the thresholds, and EM_1 and EM_2 are error monitor functions computed on the two halves of the observation window. When a critical condition is detected, the observation window length is reduced. In fact, a phasor estimation based on a shorter samples window is expected to feel later the effect of an incoming fast transient and to exit sooner from a critical condition. A shorter filter presents a wider pass-band, thus leading to a higher promptness and a lower rejection of wide-band noise. A trade-off is needed between these two aspects and, for this reason, it has been chosen to reduce the window length from four to three cycles. Thus the new phasor estimation is obtained by a further application of WLS algorithm:

$$\hat{\mathbf{p}} = \left(\widetilde{\mathbf{B}}^{\mathbf{H}}\widetilde{\mathbf{W}}^{\mathbf{H}}\widetilde{\mathbf{W}}\widetilde{\mathbf{B}}\right)^{-1}\widetilde{\mathbf{B}}\widetilde{\mathbf{W}}^{\mathbf{H}}\widetilde{\mathbf{W}}\tilde{\mathbf{s}} \tag{3.4}$$

where $\tilde{\boldsymbol{s}}$ is the new reduced window of samples. $\widetilde{\mathbf{B}}$ is obtained from $\mathbf{B}$ by suppression of the rows corresponding to the suppressed samples and $\widetilde{\mathbf{W}}$ is the new weighting matrix. In Figure 18 the flux diagram of the Adaptive TF-WLS method is shown:

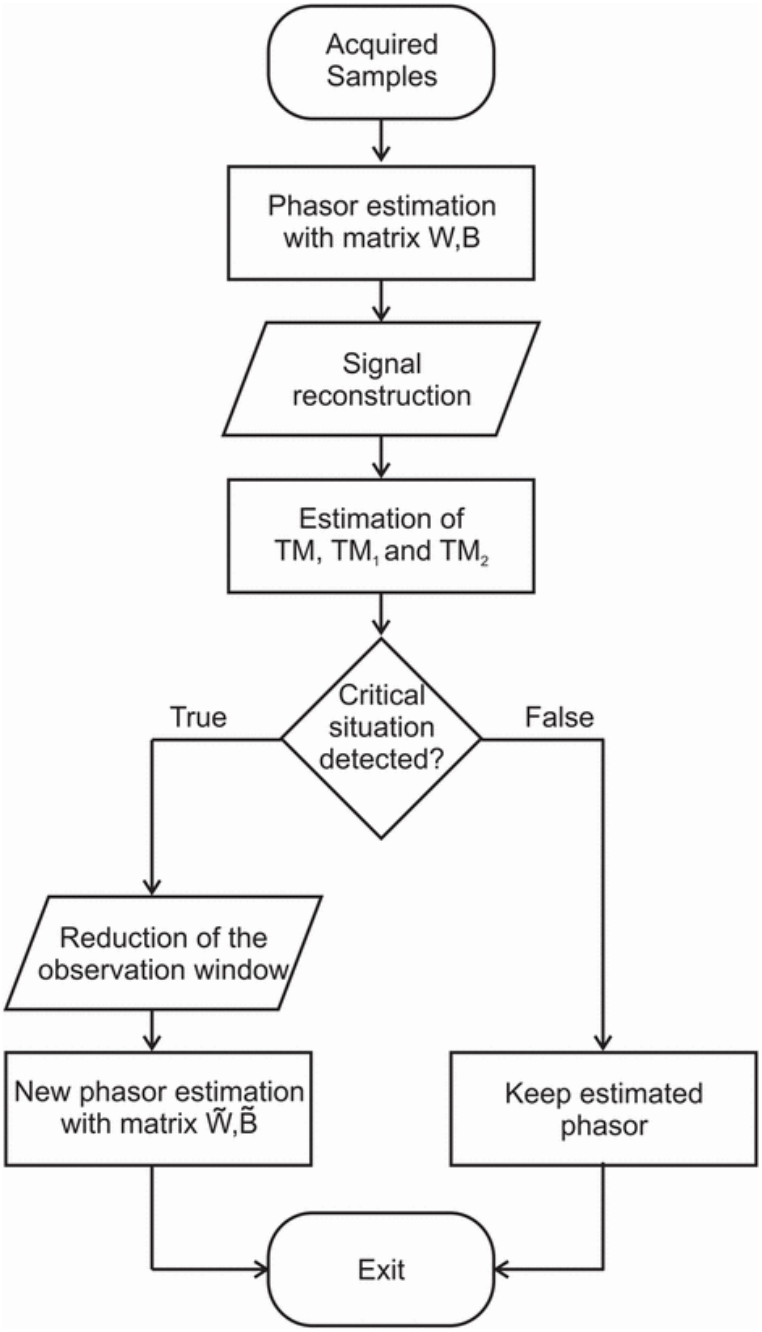

Figure 18. Flux diagram of the modified method.

The described algorithm has a general approach, that can be synthetically described as a re-weighting of the samples based on an evaluation of the first-step phasor estimation error.

3.1.2 The tests of the proposed solution

The proposed solution, referred to as Adaptive TF-WLS, is compared with other algorithms: classical DFT and TFT-WLS. Every method has been applied in a sort of sliding window approach, that is by overlapping observation windows, continuously shifting the window by a single sample. The estimated phasors are referred to their reference time, that is the centre of the observation window. The chosen sampling rate is 10 kSa/s and values α_{th} and β_{th} have

been heuristically set to 10^{-4} and $5 \cdot 10^{-4}$, respectively. The use of DFT is widespread, thus it has been used as the base method to compare with. The chosen DFT works on a one-cycle observation window, representing thus a good means of comparison for the problem at hand, because of its fast response.

Before testing the proposed method with fast transient changes, preliminary tests have been executed to show that the changes introduced in the Adaptive TF-WLS do not lead to a degradation of performance in the conditions where the classic TF-WLS algorithm. Here, only one meaningful test, relevant to an amplitude modulation, will be presented. The modulating signal has amplitude equal to 10 % of the modulated waveform and frequency equal to 5 Hz. For this test, the performances of the methods have been evaluated by means of TVE. Figure 19 shows the maximum and mean TVE (%). The results show that the Adaptive TF-WLS presents no performance degradation with respect to the classic TF-WLS. The DFT method does not perform well under such dynamic condition, because it is not able to follow signal changes that take place in the observation window.

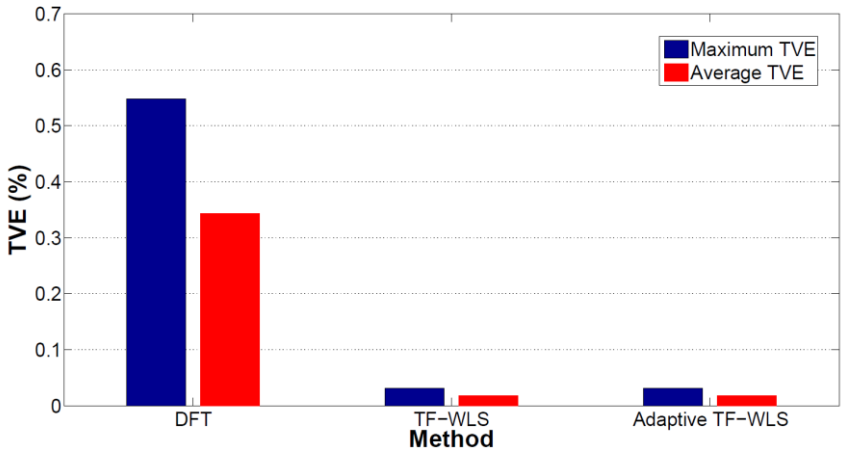

Figure 19. Maximum and mean TVE (%) values for an amplitude modulation test.

In order to study the performance of the modified method under fast transient events, some tests with step changes (amplitude and phase) have been performed. During simulations, the signal instantaneously passes from a steady-state condition to another one. Methods performances have been evaluated by means of the TVE response time.

In Figure 20, the TVE trends for a +20 % amplitude step are reported. It is possible to notice that the Adaptive TF-WLS method shows a faster response to the step than the classic TF-WLS.

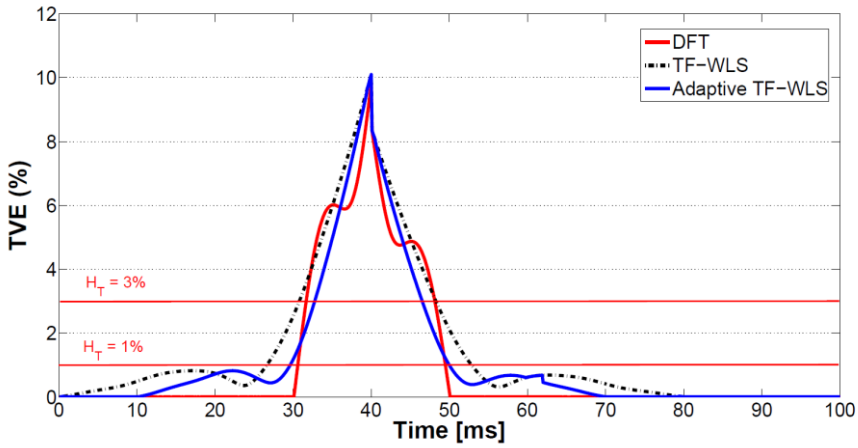

Figure 20. TVE response time for an amplitude step test of +20%.

In Table 12 the response times, for the cases of the +10% and +20 % amplitude steps, are given with HT = 1 % and HT = 3%, respectively. The Adaptive TF-WLS method seems to outperform the TF-WLS method for both the chosen thresholds. Of course, the one-cycle DFT presents a very fast response to step changes, because of its short observation window. However, the response time results of the Adaptive TF-WLS are very similar and, as it has been shown in Figure 20, DFT performance are far worse under non-stationary conditions.

Similar results are obtained for phase step changes. Figure 21 shows the behaviour of t_R for phase step magnitudes in the range 5° to 90° with HT = 1%. The response time obtained by the Adaptive TF-WLS method is always between the response time of the DFT and of the TF-WLS. It shows a strong improvement with respect to the TF-WLS up to 26 %

Table 12. Δt_r values for Ht = 1 % and Ht = 3 % for a +20 % and a +10 % amplitude step test.

Algorithms	**Step +20 %** Δt_R(ms)		**Step +10 %** Δt_R(ms)	
	HT = 1 %	**HT = 3 %**	**HT = 1 %**	**HT = 3 %**
DFT	19	17	18	7
TF-WLS	26	18	22	9
Adaptive TF-WLS	20	14	17	7

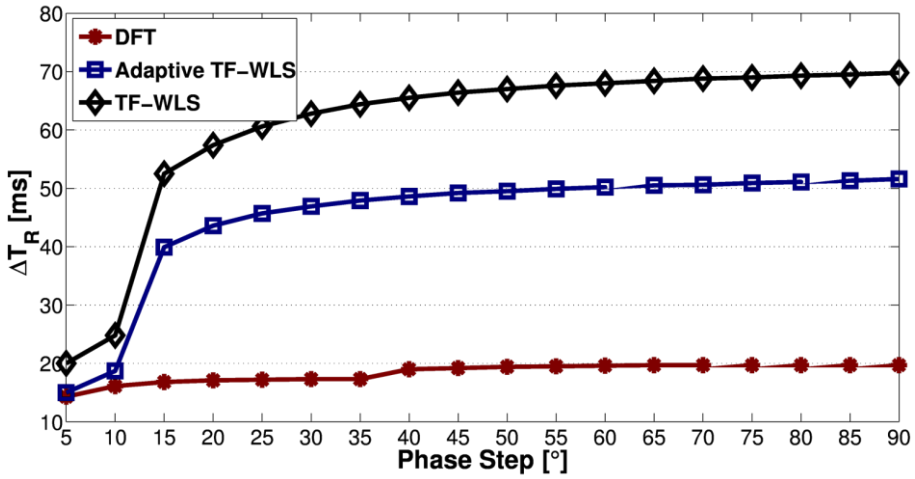

Figure 21. Δt_R for H_T = 1 % for a positive phase steps from +5° to +90°.

Figure 22 shows the TVE dynamics in case of a phase step of +45°. It is clear that the Adaptive TF-WLS method is much faster than the original one.

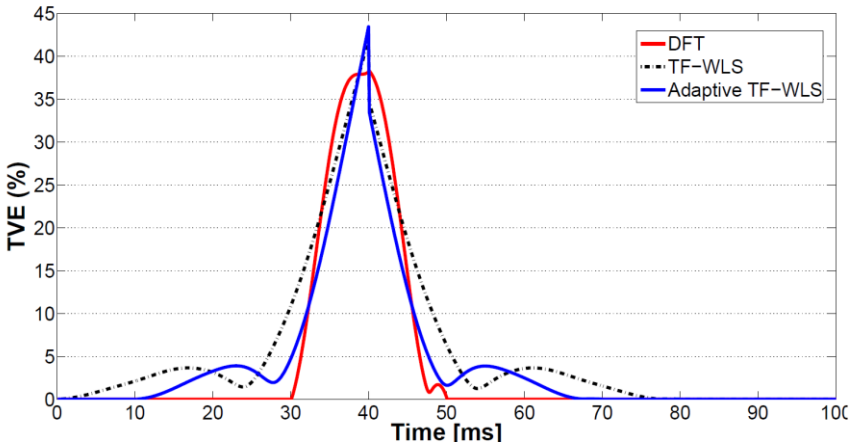

Figure 22. TVE response time for an phase step test of +45°.

To further study the performances of the proposed method, a series of tests where different conditions were simulated simultaneously have been performed. The goal of these tests is to highlight the behaviour of the proposed algorithm when an undesired disturbance like a step change is overlapped to dynamic evolutions that need to be observed. As an example, Table 13 shows the results of two tests in presence of harmonics and off-nominal frequency. In both cases, the simulated signals are affected by the presence of forty harmonics, with a Total Harmonic Distortion (THD) equal to 10 %. The sinusoidal signal at off-nominal frequency undergoes an amplitude step change of 10 % in the first test, whereas a phase step change of 10° is used in the second one.

Table 13. t_r results for tests in presence of step changes and harmonics at off-nominal frequency equal to 52.5 Hz.

Algorithms	Step +10% Δt_R(ms)		Step +10° Δt_R(ms)	
	HT = 1%	HT = 3%	HT = 1%	HT = 3%
DFT	- -	-	-	-
TF-WLS	21	9	27	17
Adaptive TF-WLS	15	9	24	14

Once again the Adaptive TF-WLS method outperform in all the situations the classic TF-WLS algorithm, showing an improvement up to 29 %. Table 13 and Table 14 do not show the results for the DFT algorithm because TVE % exceeds 3 % even during steady state conditions due to the off-nominal frequency. Thus, in this cases, it is not possible to determine the response time for the DFT. In the last series of tests, an amplitude and phase modulation has been added to the step changes and the harmonic content described in the previous tests. The modulating signal is characterized by $k_x = k_a = 0.1$ and modulating frequency $f_m = 5$ Hz. Table 14 shows the results of the two proposed simulations. The results are almost identical to those obtained in the previous tests, highlighting that the proposed method works fine also when different disturbances occur.

Table 14. tr values for tests where a step change and harmonics are superimposed on amplitude and phase modulation at off-nominal frequency equal to 52.5 Hz.

Algorithms	Step +10% Δt_R(ms)		Step +10° Δt_R(ms)	
	HT = 1%	HT = 3%	HT = 1%	HT = 3%
DFT	- -	-	-	-
TF-WLS	21	9	24	16
Adaptive TF-WLS	19	9	23	13

In conclusion, the tests show that, even with this simple solution, the proposed algorithm has better performances with respect to the classic TF-WLS in term of TVE response time, when the observed signal is affected by fast transient.

3.2 The P+M synchrophasor methods

The limits of the solution presented in the previous section are the high computational burden, due to the recalculation of the coefficients matrix when a step change condition occurs, and the relatively high latency for high reporting rates.

Thus, further advancements have been proposed for this solution, driven by the idea that is possible realize a single algorithm, in the same time, compliance with the P and M classes. The proposed method is aimed at having a high level of accuracy for measurement applications while also ensuring the ability to adapt to fast transients. Frequency and its rate of change (ROCOF) are also considered since they are typical PMU outputs along with the three phasors (one for each phase). Figure 23 summarizes the proposed PMU diagram.

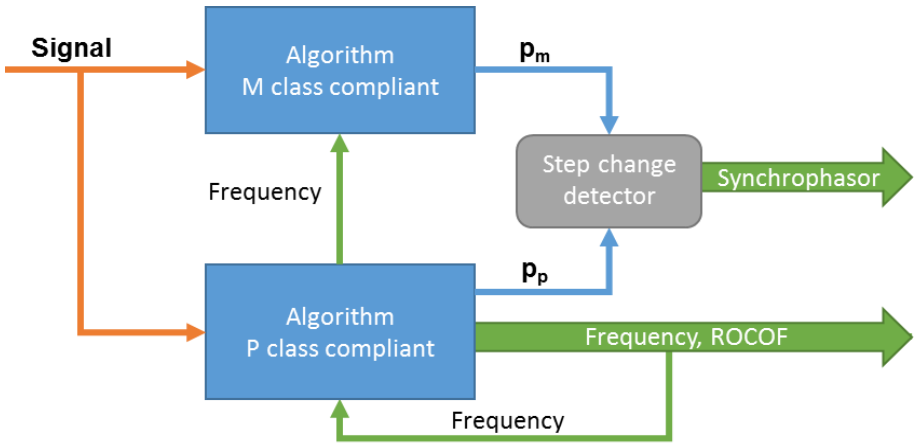

Figure 23. Diagram of the proposed solution.

The underlying idea to obtain a faster response to abrupt dynamic changes of phasors, like amplitude or phase steps, is to detect transients by means of the 2-nd order Taylor-Fourier estimation outputs, relying on the sudden mismatch between the signal and the chosen model, and then adapting the estimation algorithm to the occurring condition. Two different weighting matrices are thus used to obtain in parallel two estimates of the phasor vector $\mathbf{p}$, denoted as $\mathbf{p}_m$ and $\mathbf{p}_p$. In particular, two different Kaiser windows (with different coefficients) and the window length of 3.9 and 3.8 cycles at nominal frequency respectively, have been used.

The recognition of a fast transient is achieved with a transient detector (or step change detector as well) that detects rapid changes of the dynamic values that compose $\mathbf{p}$ (amplitude, phase and its derivatives). A new step change detector, that uses directly the different parameters provided by the estimation of the dynamic model of the algorithm, is adopted. In particular, the estimates of the first and second derivatives of the phasor amplitude and phase angle are used to achieve the correct recognition of transients.

Thus, the transient detector allows choosing the best synchrophasor estimation, $\mathbf{p_m}$ or $\mathbf{p_p}$, for each operating condition for the compliance with the M and P classes of the standard, respectively.

For the frequency and ROCOF estimation, the phase derivatives obtained from the TF outputs $\mathbf{p_p}$ are used. At the same time, the estimated frequency is used as a feedback variable (as done, for example, in [34]) for frequency tuning of the phasor estimator to enhance the estimation. Frequency estimation is also used to avoid extreme off-nominal frequency condition for phasor estimation.

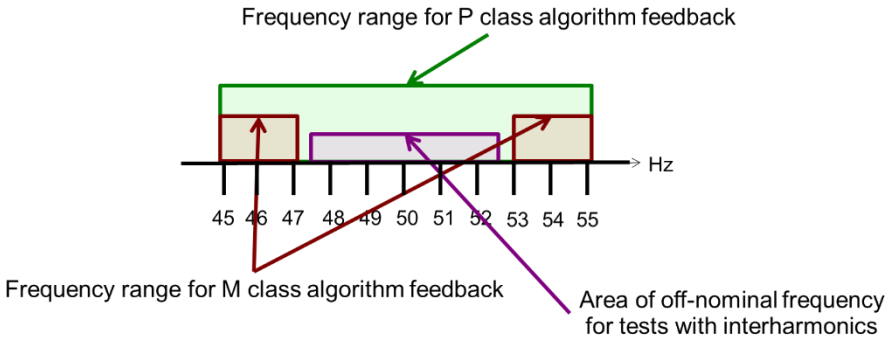

Figure 24. Frequency feedback area.

The frequency output of the P class compliant algorithm is used to enhance the phasor estimation for both classes. To avoid excessive computational burden, 11 pre-computed matrices are stored (corresponding to discrete frequencies with a 1 Hz step in the range suggested for M class, 45 to 55 Hz , as in Figure 24). The projection matrix then changes accordingly to frequency feedback in such a way that is sufficient to keep the maximum errors of the frequency estimator under the required limits. The ROCOF estimation is also obtained by the second derivative of the phase angle from the P-class estimation path.

The possibility to choose the best matrix dependently from the frequency is exploited in a different way for the two algorithms P and M. While the P algorithm tuning is used in the full range 45 Hz to 55 Hz, the M algorithm uses another policy. The M algorithm is tuned in frequency in a more limited range, from 45 Hz to 47 Hz and from 53 Hz to 55 Hz and does not change instead in the range from 48 Hz to 52 Hz. The purpose is to reach a compromise between optimal measurements in off-nominal conditions and a good rejection of the out of band disturbances, when strict latency requirements are given.

It is important to highlight that every element in the schema of Figure 23 is able to operate on a single phase basis, without merging the three phase signals. This allows the straightforward use of the proposed PMU in power distribution systems with unbalanced conditions.

3.2.1 The tests of the proposed solution

In this section, the simulation results of the compliance tests for the proposed algorithm according to the standard of synchrophasor are presented. The sampling frequency is set to 10 kHz, while a reporting rate of 50 phasors per second is considered.

In the following, subsections are dedicated to both steady state and dynamic tests, and the results are reported in terms of maximum percent TVE for the phasor estimation and of maximum errors for frequency and ROCOF, as required by the standard specifications. For some tests, to have an insight of the behavior of the algorithms, richer results are shown.

3.2.1.1 Steady state compliance tests

The results of the tests under the off-nominal frequency conditions, expressed in terms of Total Vector Error (TVE), are reported in Table 15 for the P and M classes. It is shown that the proposed algorithm can achieve all the required specifications for both classes.

The results of the tests at nominal frequency, when amplitude and phase shift are changed, are not reported because the errors are negligible, Besides, such tests are more suitable to stress a real PMU (for instance for different input levels) than just the measurement algorithm. In fact they are useful in particular to the test the other components of the PMU.

For the single harmonic test only the results for the second, third and fourth harmonics are shown in Figure 25, since these three harmonics are the closest ones to the fundamental component and thus cause the largest errors. With the proposed algorithm the harmonics are well attenuated and very low TVE is achieved. It is important to notice that the reference condition of the harmonic distortion test for M class is ten times higher than that for the P class test: this justifies the higher errors obtained in the M class test.

Table 15. Steady State Compliance Tests for Off-nominal frequency.

Test	Range	TVE Limit	Max TVE of the estimated phasors
Signal frequency range for P class	± 2 Hz	1%	0.03 %
Signal frequency range for M class	± 5 Hz	1%	0.3 %

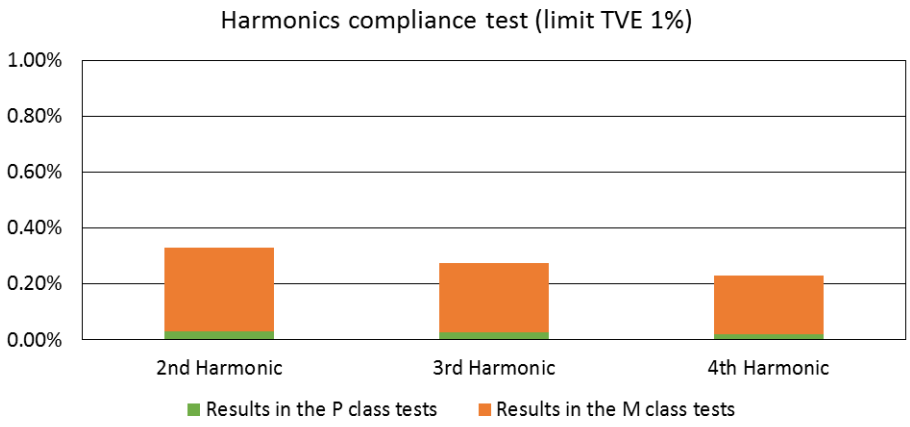

Figure 25. Steady state compliance test for harmonic rejection.

Figure 26 shows the results of the proposed method in presence of out-of-band interfering signal in three different cases for the signal frequency (f_0 = 50 Hz, 47.5 Hz, 52.5 Hz). To demonstrate the property of disturbance rejection of the algorithm, the frequency of the interfering signal is varied in two different ranges: from 0 Hz to 25 Hz and from 75 Hz to 100 Hz.

The results are described from two point of views: in terms of both maximum TVE %, among all interfering signals, and average TVE %. The average has been obtained spanning the frequency of the interharmonic with a very slow ramp, to automate the test. The results show that, in the frequency range proposed in synchrophasor standard for the reporting rate equal to 50 phasors/s, the TVEs achieved by the proposed algorithm are always below the limit (even if they are quite close to the limit for few specific interharmonic frequencies). These results are the effect of a compromise that was necessary in order to achieve both a good rejection of out-of-band disturbances, required from the M class, and a low value of latency, required for P class compliance, which will be discussed in the next subsection.

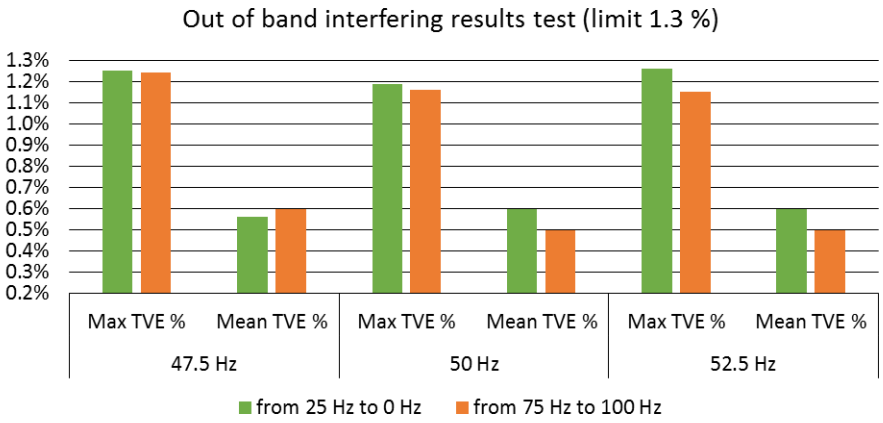

Figure 26. Steady state compliance test for out of band interfering signals.

Table 16 and Table 17 indicate the excellent performance of the frequency and ROCOF estimation for P class achieved by the proposed method under steady state conditions: the maximal values of the frequency estimation errors (FE) and ROCOF estimation errors (RFE) are one or more orders smaller than the requirements of the standard.

Table 16. Steady State Frequency Compliance Test for P Class.

Tests	Range	FE Limit	Max FE of the estimated frequency
Signal frequency	± 2 Hz	0.005 Hz	$2.0 \cdot 10^{-4}$ Hz
Harmonic distortion (single harmonic)	1% up to 50^{th}	0.005 Hz	$6.2 \cdot 10^{-4}$ @100 Hz $2.2 \cdot 10^{-5}$ @150 Hz $3.9 \cdot 10^{-5}$ @200 Hz

Table 17. Steady State ROCOF Compliance Test for P Class.

Tests	Range	RFE Limit	Max RFE of the estimated ROCOF
Signal Frequency	± 2 Hz	0.01 Hz/s	$7.5 \cdot 10^{-5}$ Hz/s
Harmonic distortion (single harmonic)	1% up to 50^{th}	0.01 Hz/s	0.004 Hz/s @100Hz 0.005 Hz/s @150Hz 0.004 Hz/s @200Hz

It is important to highlight that the proposed frequency and ROCOF estimator is compliant with the P class but the good results in off-nominal are confirmed for a wider range of frequencies and allow to use the frequency estimator in the range ± 5 Hz around the fundamental. However, the results in presence of out of band interference signal do not permit to extend the compliance

to M class. These problems are discussed in literature, both for simulations [34] and real applications of PMUs [35] and represent a goal to reach for a complete compliance for the classes P and M.

3.2.1.2 Dynamic compliance tests

The tests with modulated signal and with frequency ramp have been carried out for both P and M classes. The TVE limits for these tests are 1 % for the frequency ramp and 3 % for the modulated signals for both classes.

As shown in Figure 27, two different types of modulation are used: a phase and amplitude modulation with an amplitude modulation index kx equal to 0.1 (modulating signal is 10 % of the carrier amplitude) and a phase modulation index ka equal to 0.1. For the tests, to stress the dynamic responses of the algorithm, the maximum modulation frequencies suggested in the standard are used, that are 2 Hz for the P class and 5 Hz for M class. Figure 27 shows that the limit of 3 % is widely respected under both the modulation cases.

For frequency ramp tests, following the standard, a frequency variation rate equal to 1 Hz/s is used for the two frequency ranges: from 45 Hz to 55 Hz for M class and from 48 Hz to 52 Hz for P class. In both cases the maximum achieved TVE % is under the required limit.

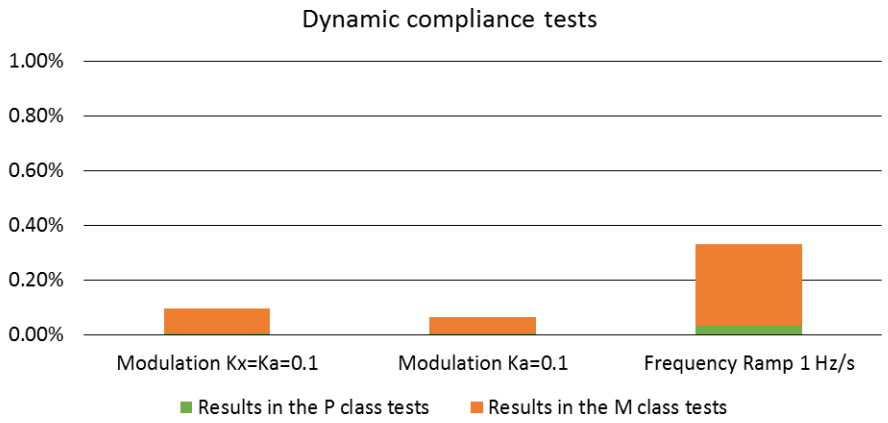

Figure 27. Dynamic compliance test for modulated signals and frequency ramp.

Table 18 and Table 19 show the results for frequency and ROCOF estimation during the aforementioned dynamic tests of modulation and ramp. The maximum errors are under the limits imposed for the modulation cases. They are also very small for the frequency ramp, confirming that the frequency tuning in the proposed method is sufficient to meet the strict limits imposed for the P class.

Table 18. Frequency Estimation under Modulated Signal and Frequency Ramp Tests for P Class.

Tests	Range	FE limit	Max FE of estimated frequency
Modulation AM+PM	fm = 2 Hz; ka=kx=0.1	0.06 Hz	0.002 Hz
Modulation PM	fm = 2 Hz; ka= 0.1	0.06 Hz	0.001 Hz
Linear Frequency Ramp	+/- 1 Hz/s 48 – 52 Hz	0.01 Hz	$2 \cdot 10^{-4}$ Hz

Table 19. ROCOF Estimation under Modulated Signal and Frequency Ramp Tests for P Class.

Tests	Range	RFE limit	Max RFE of estimated ROCOF
Modulation AM+PM	fm = 2 Hz; ka=kx=0.1	3 Hz/s	0.04 Hz/s
Modulation PM	fm = 2 Hz; ka= 0.1	3 Hz/s	0.02 Hz/s
Linear Frequency Ramp	+/- 1 Hz/s 48 – 52 Hz	0.1 Hz/s	0.002 Hz/s

The step change test is performed for the P class, that defines much stricter specifications for this test than the M class. The results for response time and maximum overshoot for synchrophasor estimation are shown in Table 20 and confirm that the proposed algorithm complies with the requirements of the P class and, consequently, also for the M class.

Table 20. Synchrophasor Estimation under Step Change Test for P Class.

Tests	Range	Response time		Max overshoot	
		limit	results	limit	Results
Magnitude step change	+10 %	34 ms	20 ms	5 %	4.51 %
	-10 %		19 ms		4.50 %
Phase step change	+10°		22 ms		4.51 %
	-10°		22 ms		4.50 %

Table 21 and Table 22 show the results for the frequency response time and for the ROCOF response time, that are compliant for all the cases provided by the standard.

Table 21. Frequency estimation under Step Change Test for P Class.

Tests	Range	Frequency Response time	
		limit	results
Magnitude step change	+10 %	70 ms	59 ms
	-10 %		60 ms
Phase step change	+10°		62 ms
	-10°		62 ms

Table 22. ROCOF estimation under Step Change Test for P Class.

Tests	Range	ROCOF Response time	
		limit	results
Magnitude step change	+10 %	80 ms	74 ms
	-10 %		74 ms
Phase step change	+10°		73 ms
	-10°		73 ms

As for the latency, the proposed estimator may introduce a maximum value of 39 ms, while the limits imposed by the standard for a reporting rate of 50 frames/s are 40 ms and 100 ms, respectively, for classes P and M.

The delay time is defined as the “interval between the instant that step change signal is applied to the input of a PMU and measurement time that the stepped parameter achieves a value that is halfway between the initial and final steady-state values”. In this case the maximum delay resulted by the proposed algorithm is negligible with respect to the maximum value required by the standard which is 5 ms for a reporting rate equal to 50 frames/s.

In the Table 23 a summary of compliance for the proposed methods is shown. It is easy to see that the only two tests in which the results are not compliant to the standard are the frequency and ROCOF measurement in the out-of-band cases; it is important to highlight that the out-of-band limits are far stricter than limits in presence of harmonics. However, the method is completely compliant for the P class for synchrophasor, frequency and ROCOF and for P and M classes simultaneously for synchrophasor measurement.

Table 23. PMU Tests: summary of compliance.

	Steady State					Modulation/Ramp				Step Change				Latency
	P class		M class			P class		M class		P class		M class		P class (< M)
	ON	H	ON	H	OOB	MOD	RAMP	MOD	RAMP	a	φ	a	φ	
Synchrophasor	✓	✓	✓	✓	✓	✓	✓	✓	✓	✓	✓	✓	✓	✓
Frequency	✓	✓	✓	✓	✗	✓	✓	✓	✓	✓	✓	✓	✓	✓
ROCOF	✓	✓	✓	✓	✗	✓	✓	✓	✓	✓	✓	✓	✓	✓

- ON: off-nominal
- H: harmonic disturbance
- OOB: out-of-band interference
- MOD: modulation

3.3 A PMU for electrical distribution networks

The algorithm proposed in the previous section was implemented in a device during a collaboration between University of Cagliari and the E.On Energy Research Centre, Institute for Automation of Complex Power Systems of Aachen in Germany.

The topic of the project is to realize a prototype of PMU for the electrical distribution networks able to respect the main following constraints:

1. High level of accuracy: in an electrical distribution networks the distance are lesser than in the electrical transmission networks and this means that the angle's difference between two points of the network could be very small and difficult to measure with a PMU designed for transmission.
2. Low cost: the high price of the PMU currently on the market leads to the use of a reduced number of devices only in transmission networks. Nowadays the price is getting lower but the usual price is still far from what required for a deep use of these devices in the distribution networks. The idea is to use low cost devices so that the final PMU price should be about half the price of the cheapest commercial PMU.

3. Easy implementation of the prototype: indeed, generally, the time to realize a project is a critical factor and thus the hardware chosen for the prototype should be easy to program and to upgrade for any new functionality.

To respond at the three main constraints, a solution from National Instruments, the CompactRIO, was adopted. The devices (Figure 28) is composed by:

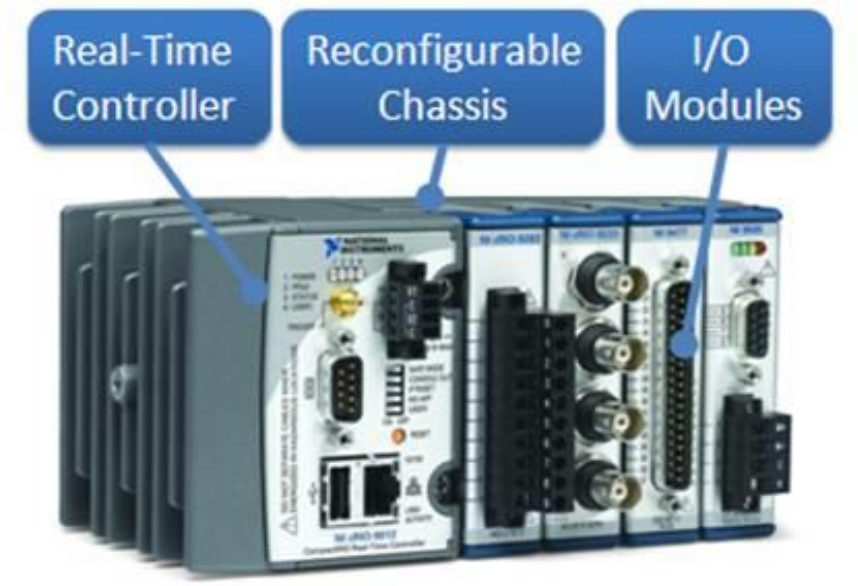

Figure 28. The scheme of the CompactRIO device from National Instruments.

- A fast real-time controller: the controller is the brain of the system, because inside the controller the different algorithms proposed can run to obtain the measure of synchrophasor, frequency and ROCOF. Moreover, the fast Ethernet ports permit to control the device and, in the same time, to send all the measured data to a PDC compliant with the standard IEEE C37.118.2. One USB port in the controller is used to store the synchrophasor locally.

- A reconfigurable chassis with FPGA module: with the chassis, the prototype is ready to work in the field without other particular expedients. Moreover, in the chassis a configurable FPGA module permits to achieve high level of accuracy in time critical applications.

- I/O modules: the I/O modules are able to extend the potentiality of the prototype with new functions. Generally, it is possible to use more than four boards at the same time. The communication between the microcontroller and the I/O modules is through the FPGA channels to permit a fast communication. Other techniques

are present to control the I/O boards (scan mode) but are not able to respect the strict constraint of communication speed requested by the synchrophasor measurement.

Following the normal scheme of a PMU, the prototype is designed with the following requirements:

- Acquisition of 6 different signals (three phase currents and three phase voltages) simultaneously with high resolution and high sampling frequency to obtain more accurate measurements and to evaluate more electrical phenomenal with high frequency.
- Time synchronization provided by a GPS module and a GPS antenna.
- Communication system based on the standard IEEE C37.118.2 to send the measured synchrophasors to recorder devices.
- Capability to report up to 50 measures per second, the maximum reporting rate suggested from the standard.
- Capability to send alarms in the case of magnitude, frequency of ROCOF crossing of chosen threshold levels.

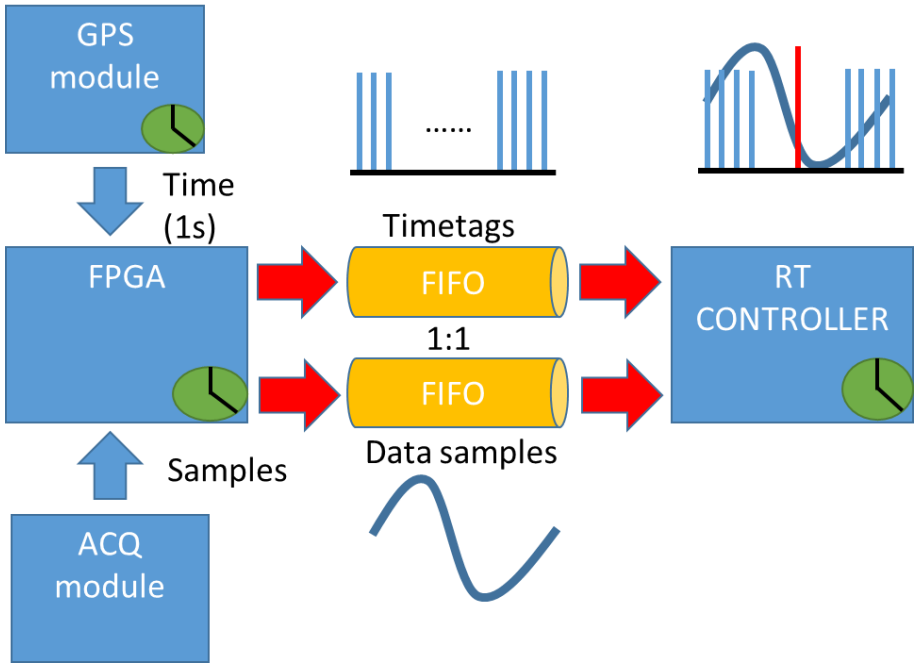

Figure 29. Scheme of the PMU prototype.

In the Figure 29 the different parts of the PMU prototype are shown. The GPS module and the acquisition modules acquire the information of respectively time and electrical quantities of

interest to the FPGA that keeps the relation between samples and time. Two different deterministic FIFOs permit to share the data from the FPGA to the real-time micro controller. The microcontroller takes the data from the FIFO dependently of the reporting rate set on the device. In the microcontroller, before the estimation of the synchrophasor an alignment of the time tags and samples permits to choose the correct value of the time reference at the centre of the window.

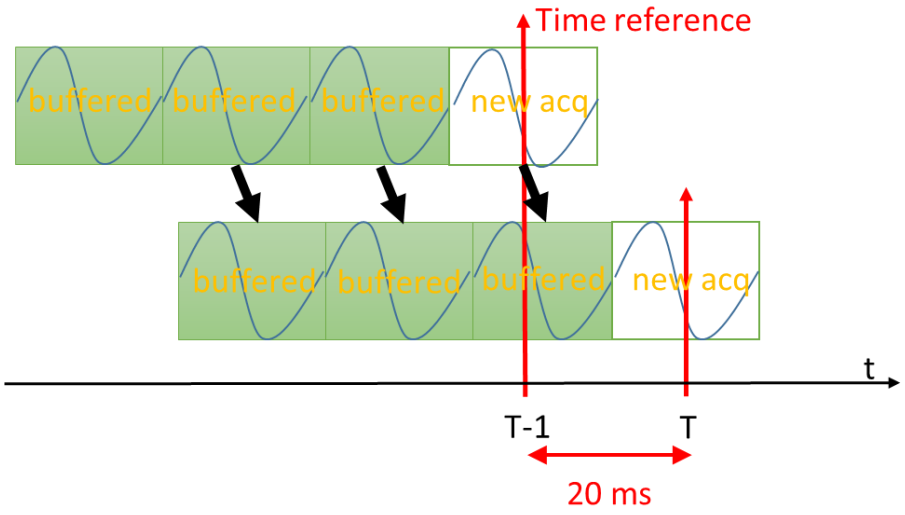

Figure 30. Data set of the acquired signal.

The Figure 30. shows how the data are stored in the microcontroller before the computation of the algorithm. Every cycle, at the nominal system frequency (20 ms at 50 Hz), a new set of data is used with other three cycles recorded before, using an overlapping technique. The algorithms implemented are a modified version of the Adaptive TF-WLS presented in 3.1.1. and another algorithm presented in [49]. The computational cost required to obtain the measurements strictly depends on the reporting rate and the sampling frequency that is directly connected to the number of samples evaluated by TFT. The hardware of NI CompactRIO chosen for this project permits to use the same algorithm for current and voltage measurements.

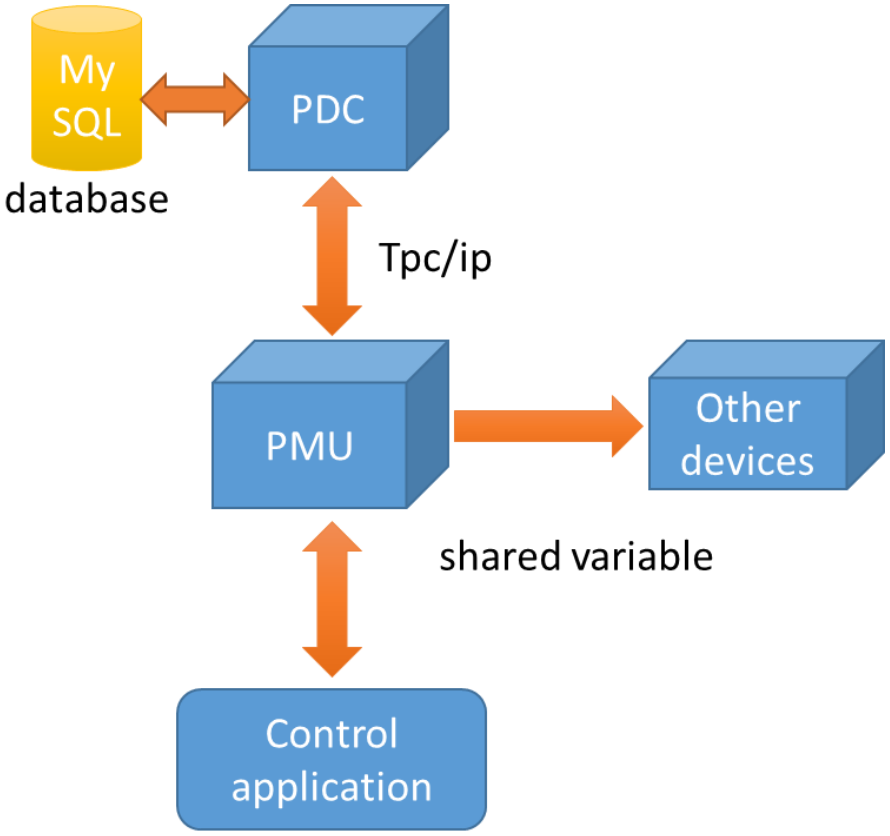

Figure 31. The communication system of the PMU prototype.

The communication is a key element of a commercial PMU. In the Figure 31 a general scheme of communication between the PMU prototype and other devices is shown. The normal communication between the PMU and the PDC is compliant with the IEEE C37.118.2. In the project, the communication protocol TCP is chosen. To extend the communication of the PMU to other devices the shared variables from National Instruments are implemented in the PMU prototype. The shared variables are information stored in the prototype that are optimized for the National Instruments hardware. For the project two different applications use the shared variables to read the information about the measurement (synchrophasor, frequency, ROCOF, alarms and others data) and to update information in the PMU prototype as new alarm levels or to change the algorithm before the start of the device.

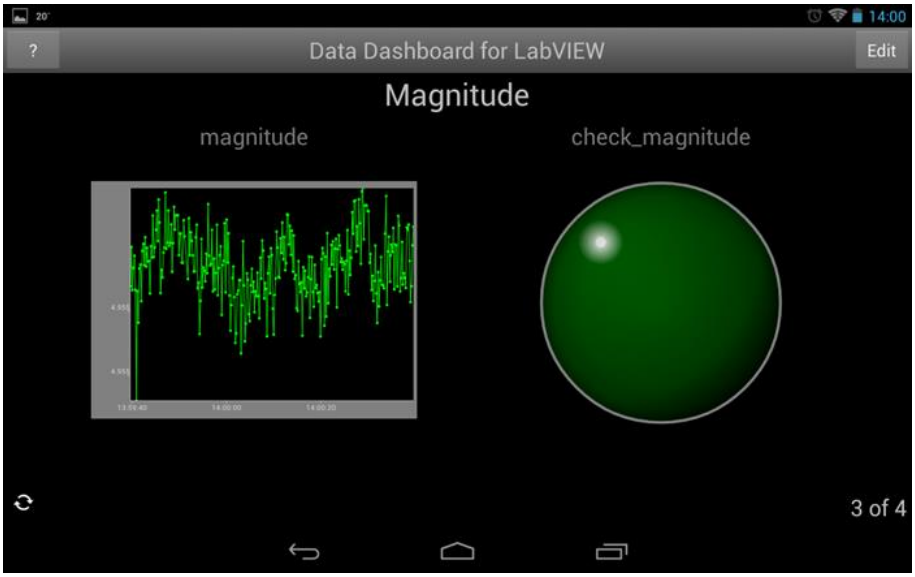

Figure 32. Data Dashboard from National Instruments to receive the shared variables from the PMU prototype.

Figure 32. shows the Data dashboard, an application from National Instruments to communicate with the PMU through the shared variables. The software permits to control and receive the data from the PMU prototype with different devices like tablet and mobile phones present in the same network of the PMU. This can be helpful to easily set up the PMU without connecting cables.

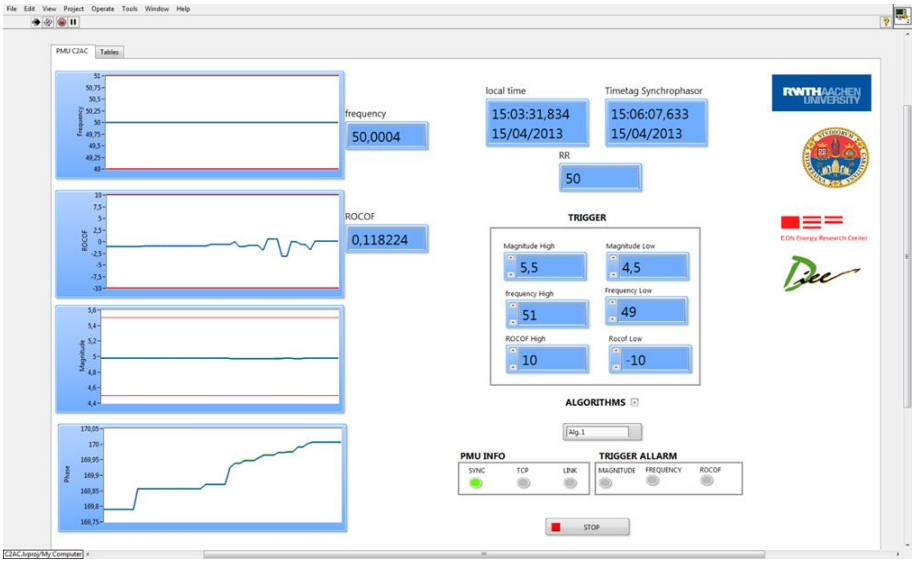

Figure 33. User interface software to control the PMU prototype.

The software to control the device and to receive the data, written in LabVIEW, is shown in Figure 33. It permits to choose the algorithm to perform the measurement on the PMU prototype and to set the threshold levels for magnitude, frequency and ROCOF alarms. The program is able to set the parameters of interest in the PMU but also to receive the measurements like a PDC. In the Figure 34, the PMU prototype implemented with the CompactRIO hardware

is shown when under test with three signal generators. It is possible to see the two I/O acquire boards and the synchronization board is present. A free slot is present for future upgrade of the system.

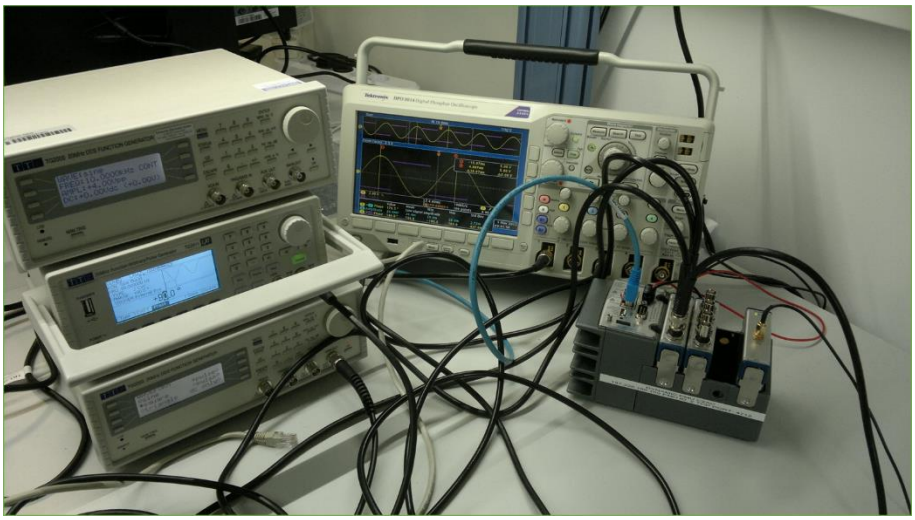

Figure 34. The PMU prototype under the synchronization test with different signals.

4 A distributed PMU for the electrical substations

This chapter presents a new distributed architecture to measure synchrophasors in power substations, inspired by the standards IEC 61850. The new scheme is implemented in the process bus, where a high performance Merging Unit (MU), synchronized by PTP (Precision Time Protocol), according to the standard IEEE 1588-2008, sends the Sampled Values (SVs) to an IED enabled to behave as a PMU. The synchrophasors are evaluated in the IED through an algorithm based on the Taylor Fourier Transform and suitably modified to have high performance. The main causes that may affect the uncertainty of the new distributed architecture are investigated in this chapter.

4.1 The distributed PMU

The rapid diffusion of Intelligent Electronic Devices began in the 1980s and '90s, when the IEDs replaced the previous, single function, instruments with multi-functional devices, thanks to the possibility to re-define the functionalities by simply redesigning the software. The IEDs communicate with each other to share and store data through the communication network. This significant change in the power substations has led to the need for a standard to regulate the changes in progress.

The IEC 61850 [36] is a series of standards that represents a fundamental basis for power substation automation systems. The standards led to a reduction of the number of cables between transducers, IEDs and MUs equipped with the network interface, which increased the reliability of the system [37].

As aforementioned, the synchrophasors are measured, according to the standard, by means of PMUs and are sent and stored into the PDCs . The PMU was originally designed to be a stand-alone instrument where signal acquisition, synchronization, estimation and communication are integrated in the same device.

On the other hand, according to the concepts proposed by the IEC 61850, the different functions can be separated in different devices inside the substation, by acquiring voltage and current signals through suitable transducers and a MU and leaving to the IED the functionality of synchrophasors estimation [38]. This possibility, which reduces the costs for safeguarding the reliability and can be defined as a PMU- enabled IED, according to [39], has been firstly explored in [40]. In the proposed solution, the MU acquires and digitizes the signals appropriately converted by suitable voltage and currents transducers. The digital SVs are tagged with the

reference time and are sent through a process bus to the IED, where the algorithm to evaluate the synchrophasor is implemented.

4.1.1 The standard IEC 61850

The introduction of IEC 61850 standard [36] has deeply changed the Substation Automation System (SAS), thanks to the introduction of a distributed control system based on network infrastructure and to an advanced object oriented description of the nodes and services forming the automation system, which promotes the interoperability between different vendors. The IEC 61850 standards provide for two different communication levels: the station bus and the process bus. The former typically interconnects the SCADA control system to the bays forming the primary substation. The latter links instrumentat transformers, protections and MUs to the IEDs on the bay. The two infrastructures have different requirements and thus the technologies and architectures adopted to deploy the two buses are usually different. Typically the station bus is implemented using a performing fibre optical gigabit Ethernet, with a ring topology to improve the availability of the communication. On the contrary, the process bus has to manage a larger amount of data coming from instrument transformers or MU deployed on the substation for protection and monitoring applications. Therefore, usually 1/10 gigabit Ethernet network is adopted to satisfy these requirements.

The IEC 61850 maps the more demanding services at Ethernet Level to reduce the propagation delay of packets over the network infrastructure. The data sampled by the instrument transformers equipped with digital interface or by the MU are mapped at Ethernet level as SV messages. The IEC 61850-9-2LE defines a set of guidelines to facilitate the interfacing of instrument transformers and MUs to the process bus. The IEC 61850-9-2LE defines two classes of SV rate, each of them dedicated to a specific application. The first class of SV is dedicated to protection applications: the measurement devices compliant with this profile have to sample the current or the voltage 80 times per grid cycle (for instance 50 Hz in EU and 60 Hz in USA). The instruments developed for more demanding applications, like power quality monitoring, have to sample the measurand 256 times per grid cycle. According to this guideline, the MUs or the instrument transformers have to be synchronized to each other, in order to achieve a sampling accuracy below 4 μs. The synchronization of the equipment has to be obtained using a 1-PPS dedicated signal, usually recovered using a GPS receiver and distributed to each device. A sequential packet number is used to recover the sampling cycle of each instrument. However, the recent standard for the digital interface of instrument transformers, IEC61869-9, provides an

advanced synchronization mechanism of the devices based on the IEEE1588 standard . The data sampled on the grid have to be mapped in SV messages, containing the sampling time (timestamp). In this way, the receivers, usually a IED, can easily recover the stream of data sent by the transformers, also in the case the packet are heavily delayed by switches of the process bus.

4.1.2 The standard IEEE 1588-2008

The IEEE1588 standard defines the Precision Time Protocol (PTP), which provides for an accurate synchronization mechanism (well below the microsecond) based on a master-slave architecture. The synchronization mechanism is similar to other protocol-based synchronization techniques, like NTP. However the IEEE1588 allows obtaining more accurate synchronization since the synchronization messages are timestamped usually at hardware level, reducing the contribution due to software stack. Obviously, in a real network, all the network devices have to be able to identify the sync messages, in order to compensate the propagation delay introduced by the network. The standard defines two difference class of network devices, the transparent clock and the boundary clock. The use of dedicated network devices increases the synchronization performance of the system but can increase the cost, since it requires the replacement of old network equipment. The high synchronization performance of this protocol suggests its use in an environment different from the original one, like the power system. Recently, a dedicated IEEE1588 profile for power system, IEEE C37.238, has been approved. This profile defines a subset of requirements defined in the IEEE1588 standard dedicated to power system.

4.1.3 A distributed measurement network based on IEC 61850

As stated in the previous subsections, the IEC 61850 standards provide for two different communication levels: the station bus and the process bus.

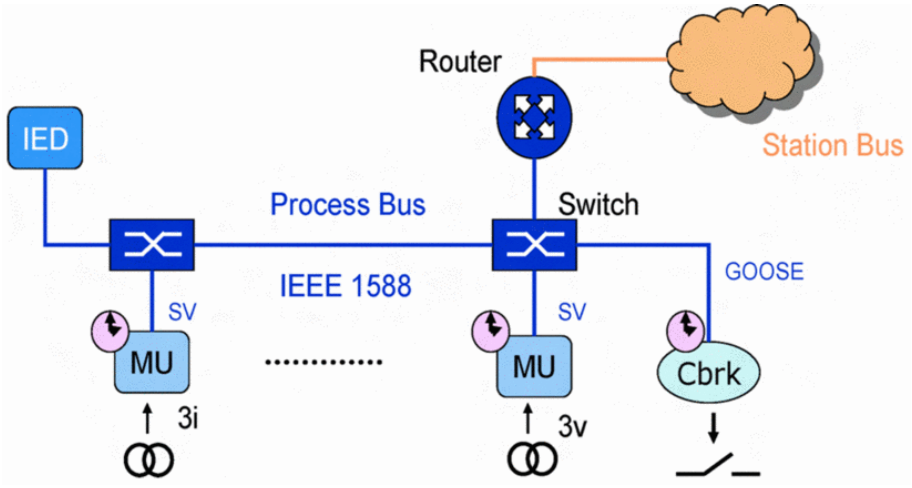

Figure 35. The proposed distributed measurement architecture based on IEC 61850.

The process bus is typically adopted to connect measurement devices, like instrument transformers, and actuators, like protections and circuit breakers, to the IEDs of the bay in a primary substation. Traditionally, these devices are directly connected to the controller of the bay by means of cabled connections. The IEC 61850 standard suggests the use of a dedicated process bus, to reduce the cabling and maintenance cost. The standard does not define the topology of the process bus: a single process bus can interconnect all the field devices of the substation or a process bus per bay could link the devices directly afferent. Mixed topologies are also allowed. The different topologies adopted are indifferent from the point of view of the system proposed, although they can influence the actual deployment of the bus. In the following, the architecture shown in Figure 35 is considered. In each bay, the process bus connects the devices placed on the power grid (IED, MU, and Breaker). The SCADA system can access the data from the process bus using a router, which avoids the flooding of SV messages on the station bus.

The process bus has been applied only in few actual systems, due to the long life cycle of the substations that limits the adoption of new technologies. However, in the new substations [41], [42], the field devices (instrument transformers, protections, breakers) are typically connected using a high performance network (1 Gb Ethernet). Therefore the transmission time of the generic object oriented substation event (GOOSE) packet in the network is below 4 ms. Moreover, the network devices support the IEEE 1588 standard [43] to achieve an accurate synchronization of instrument transformers and protections. The quantities of interest sampled by voltage and current transformers and the data are sent into SV messages to the IED. The SV packets are then used by the IED.

4.1.4 The test setup

In a distributed measurement system, the measurement accuracy is strictly related to synchronization capabilities of distributed nodes. In the proposed solution, the estimation of the synchrophasor depends on the synchronization capabilities of the IEC 61850 merging units interfaced to current and voltage transformers. In order to experimentally evaluate the feasibility of the proposed approach, a MU prototype has been developed from the University of Brescia, Department of Information Engineering. The simplified architecture of the prototype is shown in Figure 36.

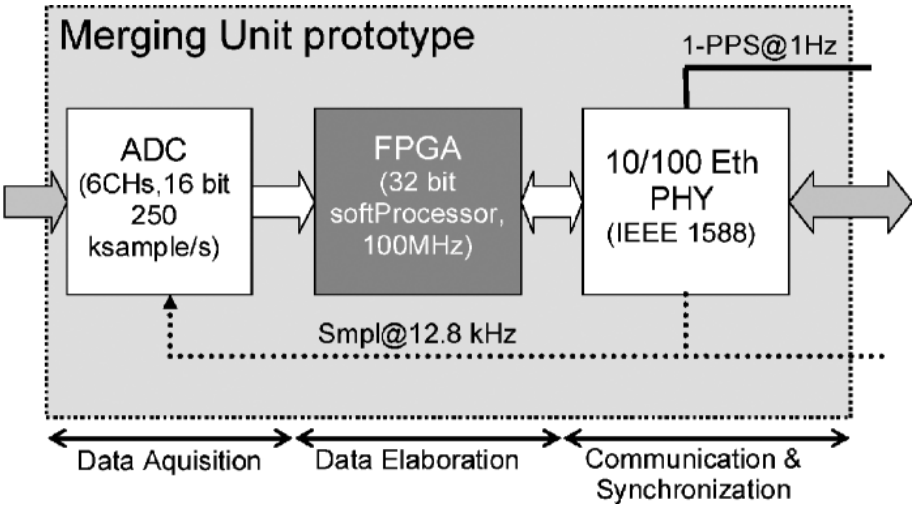

Figure 36. The architecture of IEEE 1588 Merging Unit Prototype.

4.1.5 Test results

4.1.5.1 Synchronization results

The experimental set-up has been used to characterize the synchronization capabilities of the MU prototype developed from University of Brescia, Department of Information Engineering. An IEEE 1588 master has been configured to periodically send (every 2 s) a PTP sync message over the network. Two MU prototypes (MU1 and MU2) are configured as PTP slaves. Each MU prototype generates a multicast SV packet (649 bytes) every 625 µs (about 6 Mb/s), as specified by the IEC 61850-9.2LE [44]. The two devices are connected to the master by means of an IEEE 1588 Boundary Clock (PTP BC). The MUs provide a 1-PPS output signal, in phase with their local time. The time offset between the 1-PPS signals (1-PPS_1 and 1-PPS_2) is used to estimate the synchronization uncertainty of the system. The time offset has been evaluated using the time interval measurement functionality of the counter and connecting to the channel 1 and channel 2 respectively the 1-PPS_1 and 1-PPS_2 signals, as shown in Figure 37.

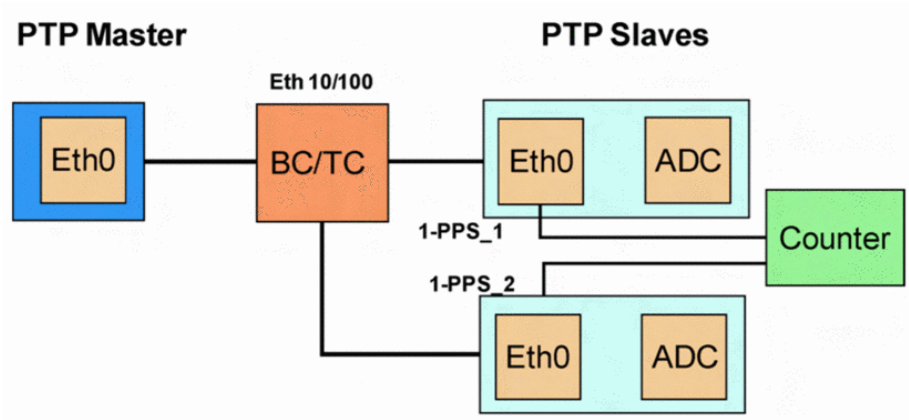

Figure 37. The experimental set-up adopted to evaluate synchronization performance of MUs.

The distribution of the time offset, over 54000 samples, is reported in Figure 38. The mean value is 4 ns and the standard deviation 11 ns. The maximum variation of the time offset, also known as jitter, is 96 ns. During the test, only the traffic generated by the MUs (about 12 Mb/s) is present on the network.

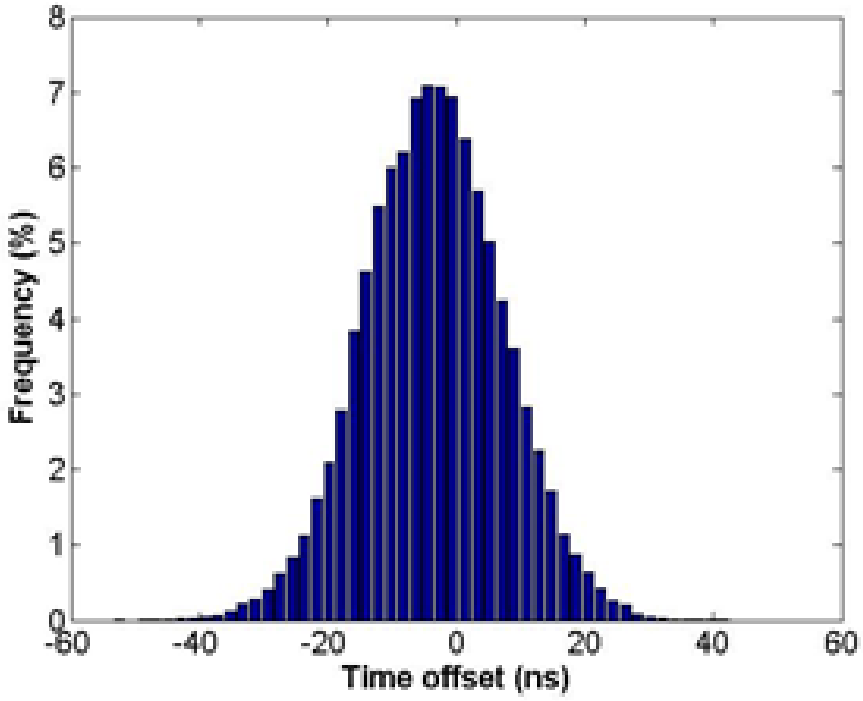

Figure 38. The distribution of the time offset between the IEEE 1588 MUs (54000 samples).

In the proposed architecture, the UTC reference time, distributed by means of IEEE 1588 protocol, is used by the MUs to assign a timestamp to hardware signals (voltage and current) on the power grid. Then, this timestamped data are used to estimate the synchrophasor. In addition, the synchronization protocol is used also to tune the local clock frequency to the reference one. The IEEE 1588 clock of the MUs is used by an internal output compare peripheral to generate a

periodic signal (12.8 kHz), which is used as sampling signal by the ADC. Since the aperture jitter of the ADC circuitry is 35 ps and the maximum aperture delay is 10 ns [48], the contribution to sampling time uncertainty due to the locally generated sampling signal may not be negligible. For this reason, the phase error, i.e. the time difference between the rising edges of two different sampling signals, has to be evaluated.

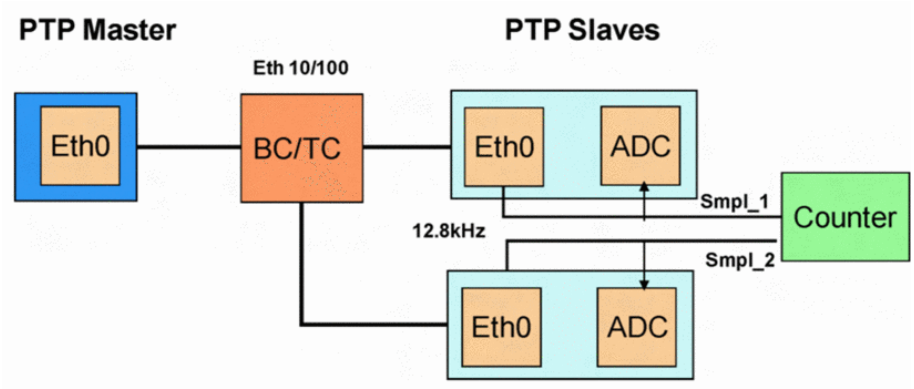

Figure 39. The second experimental set-up adopted to evaluate synchronization performance of MUs.

In the following test, the phase error between the sampling signals generated by distributed MUs has been evaluated using the experimental set-up shown in Figure 39. As in the previous experiment, the IEEE 1588 master synchronizes two MU prototypes, which are generating SV packets. At the same time, each MU generates a periodic sampling signal (Smpl_1 and Smpl_2), that feeds the local ADC. A high stability counter is used to measure the time difference between the rising edges of the sampling signals. The result of the experimental campaign, over 80 s (about 1000000 samples) is shown in Figure 40. The phase between signals generated by the MUs is affected by the synchronization performance of the system (evaluated by the previous experiment), since the output compare peripheral uses the local PTP time to generate the periodic output. Moreover, the distribution of the time offset of the sampling signals shows several peaks multiple of 8 ns, since the clock frequency of the circuitry used to generate the sampling signals is 125 MHz. As expected, the contribution to the sampling uncertainty due to phase error of sampling signal is three order of magnitude greater than the aperture jitter of the ADC.

In addition to phase error, the stability of the sampling signal has to be evaluated. The ratio between the frequency of two sampling signal has been considered as an indicator of relative frequency stability. The experimental set-up of Figure 37 has been configured for the measure of frequency ratio. The sampling signals (Smpl_1 and Smpl_2) generated by two synchronized MUs are connected to the dedicated channel of the counter. The MUs, during the experiments, are sending SV messages, as in the previous case. The distribution of the frequency ratio, measured

over an interval of one hour (3600 samples), has been reported in Figure 41. The mean of the distribution is 0 ppm and the standard deviation is on the order of 0.04 ppm. As clearly shown by the figure, the proposed system, thanks to the synchronization protocols, allows providing sampling signal whose relative frequency is highly stable, although a low cost quartz crystal oscillator (100 ppm) has been used for the development of the prototype.

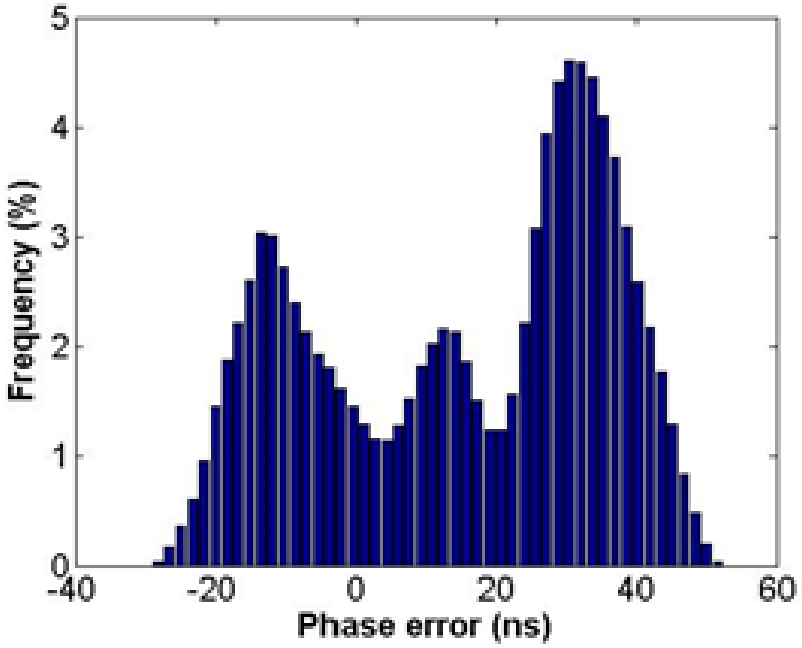

Figure 40. The distribution of phase error of the sampling signals generated by synchronized MU prototypes (1000000 samples).

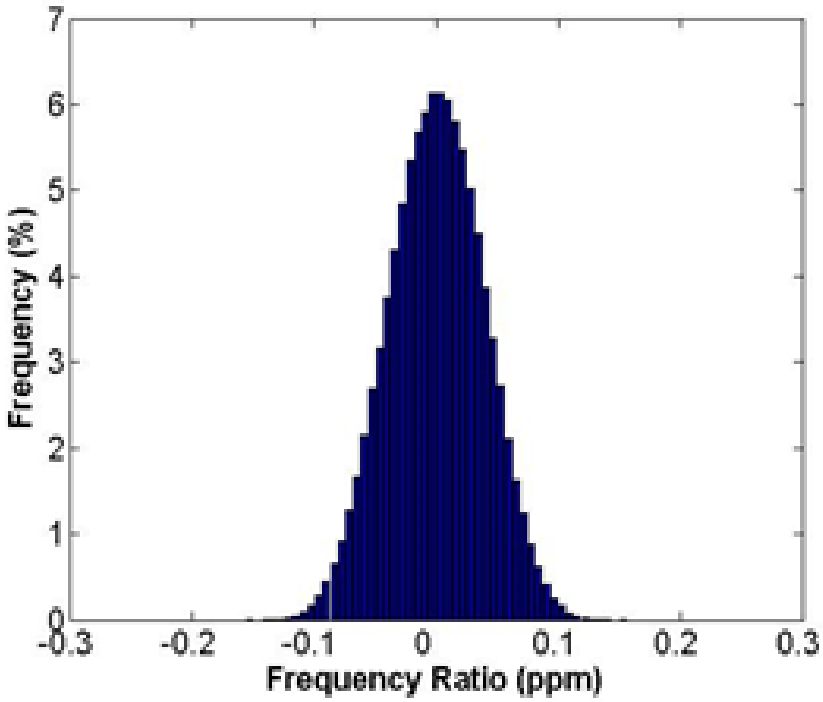

Figure 41. The distribution of the frequency ratio of sampling signals generated by two synchronized MUs.

4.1.5.2 Synchrophasor results

Simulations have been performed in order to evaluate the impact of the synchronization performance experimentally evaluated in the previous section on the synchrophasor measurement and to compare it with the uncertainty introduced by the measurement algorithm.

The algorithm used in this set of tests is the proposed method described in paragraph 3.1.1. In order to achieve the compliance also for the latency requirements, when dynamic events are detected the algorithm modifies the number of cycles from 5 to 3. Consequently, the threshold levels of the step change detector have been also modified.

The tests were performed in the simulation environment by assuming data collected at a sampling frequency of 12800 Samples/s. Each test had a minimum duration of five seconds of simulation, according to the synchrophasor standard. Furthermore, the reporting rate chosen for the simulations was 50 frame/s, in agreement with the maximum value provided in the standard, although higher values can be considered.

The values of synchronization offset obtained through experimental tests have been converted into phase errors with a simple linear relationship. These values were added to the deviations introduced by the algorithms for the estimation of the Total Vector Error (TVE).

The different types of tests that are suggested in the standard are divided into two classes: steady-state and dynamic tests. The parameter utilized to evaluate the results is dependent on the nominal frequency for the class P and on the reporting rate for the class M.

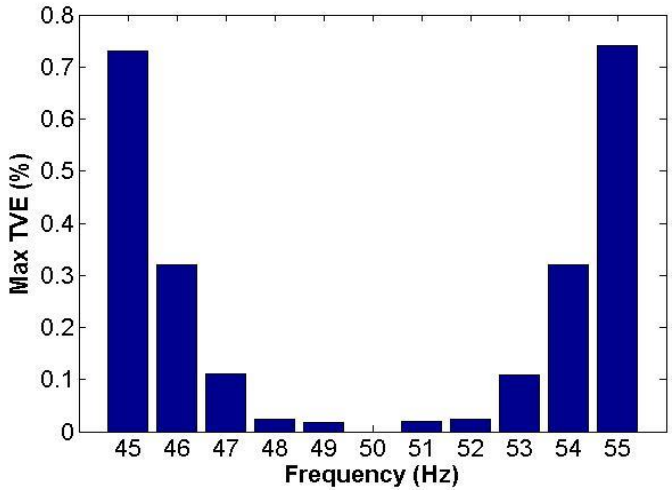

Figure 42. Test with off-nominal frequency: signal frequency range for M class and TVE % (limit 1 %).

Table 24. Maximum TVE % for harmonic distortion tests (limit 1 %).

Harmonic order	**2**	**3**	**4**	**5**	**6**
Max TVE [%]	**0.038**	**0.012**	**0.06**	**0.003**	**0.002**

Table 25. Maximum TVE % for out-of-band interference tests for reporting rate equal to 50 (limit 1.3 %).

Reporting rate [Frame/s]	**50**					
f_{in} [Hz]	49.5		50		**50.5**	
f_{oob} [Hz]	25	75	25	75	25	**75**
Max TVE [%]	**1.06**	**1.05**	**1.06**	**1.04**	**1.06**	**1.05**

4.1.5.3 Tests in steady state conditions

The results with off-nominal frequency, harmonic distortion and out-of-band interference are shown in Figure 42 and Table 24 and Table 25, respectively. The tables' captions also show the limits for each test, expressed in terms of TVE %. The method Adaptive TF-WLS fulfils the minimum values of accuracy for all frequencies belonging to the range required for the M class. Accuracy requirements for class P are less severe and do not involve out-of-band tests, and thus they are obviously complied with too. Higher TVE values could be observed in the presence of out-of-band interference if reporting rates slower than 50 frame/s were considered. These values could be reduced by appropriately modifying the weights of the samples.

Table 26. Maximum TVE % for frequency ramp tests with rate ±1 Hz/s (limit 1 %).

Range of frequencies [Hz]	**Rate [Hz/s]**	**Max TVE %**
48-52	+1	0.024
45-55	+1	0.739
52-48	-1	0.024
55-45	-1	0.740

Table 27. Maximum TVE % for amplitude and phase modulation tests (limit 3 %).

Modulation level	Modulation frequency [Hz]	Max TVE [%]
kx=0.1, ka=0	2	0.002
kx=0.1, ka=0	5	0.074
kx=0.1, ka=0.1	2	0.003
kx=0.1, ka=0.1	5	0.110

4.1.5.4 Tests in dynamic conditions

The results shown in Table 26 refer to the tests performed in the presence of a linear variation of the frequency. The maximum value of TVE % in the frequency ramp test was obtained by a variation of the signal from 45 Hz to 55 Hz at a rate of 1 Hz/s and coincides with the value obtained in the off-nominal test at 55 Hz.

Table 27 shows that the proposed method complies with the limit values imposed by the standard also for the tests in the presence of combined modulations of amplitude and phase. This is because the algorithm is based on a second order Taylor model that makes it suitable for following the trend of the phasor in the frequencies of interest.

Table 28. Response time for amplitude and phase step tests.

Step change	Response time [ms]	|Delay time| [ms]	Max overshoot [%]
Magnitude +10%	17	0.62	4.11
Magnitude -10%	18	0.62	4.20
Angle + 10°	19	0.40	4.86
Angle – 10°	19	0.94	4.85

The parameters used to assess the performance of the synchrophasor measurements in presence of magnitude or phase steps are response time, overshoot and delay time.

The Table 28 shows the results obtained by applying phase and amplitude step changes. The maximum response time should not exceed 1.70/fo, i.e. 34 ms for a system with reporting rate equal to 50 frames/s. These results show that both amplitude and phase steps are detected by the proposed algorithm, thus allowing for significant improvement in the performance.

As for the overshoot, the test with step change provides two levels of compliance for the two classes of accuracy: 5 % for the P class and 10 % for the M class. The result of the proposed

algorithm is always lower than these values and it reaches a maximum value of 4.86 % in the phase step change.

As a general comment on the results shown in this section it should be emphasized that the maximum synchronization offset registered in the experimental tests (which is in the order of 300 ns) leads to a maximum phase error of 10^{-4} rad at 50 Hz, i.e. to an equivalent TVE equal to 10^{-2} %. The impact of this deviation is therefore some orders of magnitude smaller than that introduced by the measurement algorithm and is negligible in practical situations.

4.1.5.5 Reporting latency

Latency in measurement reporting is the time delay from when an event occurs on the power system to the time that it is reported in data. The PMUs are complex measuring instruments with many different elements, each of which affects the total time of computation of the measure and, then, the latency. The latency limits are different for the two classes and depend on the reporting rate Fs, as shown in Table 29.

Table 29 Latency requirements for P and M class for the different Reporting Rate.

Reporting Rate [Frame/s]	P class [s]	M class [s]
10	0.2	0.5
25	0.08	0.2
50	0.04	0.1

In the proposed measurement system the main factors of the latency are the length of measurement window and the latency in the MU that sends the SVs. The length of the observation window is 5 cycles, i.e. 0.1 s at 50 Hz (although it changes dynamically to 3 cycles, i.e. 0.06 s, in presence of rapid signal changes). Being the time reference at the center of the window, the minimum latency is therefore 0.05 s, which means all limits defined in the synchrophasor standard can be met, with the only exception of the 0.04 s that are required for class P when the reporting rate Fs is set to 50 frame/s. On the other hand, the delay introduced by the hardware has a negligible impact on the overall reporting latency.

The results shown in this section, where the uncertainty arising from the algorithm is combined with the uncertainty of the synchronization system, clearly reveal the feasibility of the proposed distributed architecture with PTP synchronization for synchrophasor estimations, whose performance are comparable to that of a standalone PMU.

Conclusions

The synchrophasor estimation is affected by several causes of uncertainty, related to transducers, data acquisition system, synchronization system, and phasor estimation method. This work has focused on the accuracy performance of the estimation algorithm and, in particular, of the influence of the measurement model onto the performance.

In this Thesis, a comparative analysis among different algorithms through tests suggested in the synchrophasor standard is proposed. The algorithms were divided through the mathematical model in two classes: static and dynamic model. The final results of the comparative analysis demonstrated that algorithms specifically designed for dynamic phasor estimation are needed when relevant oscillations or frequency changes are present in the reference signal, but the results in term of response time were not enough to guarantee the complete compliance with the values suggested in the standard for the protection application.

With the aim to reduce time wherein the PMU estimations are outside the limits suggested by the standards and to permit a complete compliance, different solutions are proposed in this thesis. An approach based on detection of step change conditions, evaluating different levels of noise, permits to change dynamically the number of samples of the acquisition window to allow a good level of accuracy in a normal behaviour and a fast response time in presence of step changing conditions. A different approach to reduce the response time in the dynamic algorithm is called "P+M". In this approach, the respect of the classes of accuracy for measurements and protection applications is sought at the same time; this means an high level of accuracy with a low latency level, and it is possible with a different step change detection based on thresholding of derivatives of magnitude and phase of synchrophasors.

In the last part of this thesis, an innovative architecture for electrical substations was presented. The new standards IEC 61850 allow changing the usual idea of a PMU from a standalone device to a distributed device, where all the components are spread in the electrical substation. The feasibility study demonstrates that the algorithm designed for a standalone solution, tested with different signal conditions and evaluating the synchronization error introduced by the new solution , could be used in the distributed architecture compliance with the synchrophasor standard.

Publications

Journals:

1. Castello, P.; Lixia, M.; Muscas, C.; Pegoraro, P.A., "Impact of the Model on the Accuracy of Synchrophasor Measurement," Instrumentation and Measurement, IEEE Transactions on , vol.61, no.8, pp.2179,2188, Aug. 2012.
2. Castello, P.; Ferrari, P.; Flammini, A.; Muscas, C.; Rinaldi, S., "A New IED With PMU Functionalities for Electrical Substations," Instrumentation and Measurement, IEEE Transactions on , vol.62, no.12, pp.3209,3217, Dec. 2013

Conferences:

1. Castello, P.; Lixia, M.; Muscas, C., "Measurement of synchrophasors under dynamic conditions," Applied Measurements For Power Systems (AMPS), 2010 IEEE International Workshop on , vol., no., pp.1,6, 22-24 Sept. 2010
2. Castello, P.; Muscas, C.; Pegoraro, P.A., "Performance comparison of algorithms for synchrophasors measurements under dynamic conditions," Applied Measurements for Power Systems (AMPS), 2011 IEEE International Workshop on , vol., no., pp.25,30, 28-30 Sept. 2011
3. Castello, P.; Lixia, M.; Muscas, C.; Pegoraro, P.A., "Adaptive Taylor-Fourier synchrophasor estimation for fast response to changing conditions," Instrumentation and Measurement Technology Conference (I2MTC), 2012 IEEE International , vol., no., pp.294,299, 13-16 May 2012
4. Castello, P.; Ferrari, P.; Flammini, A.; Muscas, C.; Rinaldi, S., "An IEC 61850-Compliant distributed PMU for electrical substations," Applied Measurements for Power Systems (AMPS), 2012 IEEE International Workshop on , vol., no., pp.1,6, 26-28 Sept. 2012
5. Castello, Paolo; Liu, Junqi; Monti, Antonello; Muscas, Carlo; Pegoraro, Paolo Attilio; Ponci, Ferdinanda, "Toward a class “P + M” Phasor Measurement Unit," Applied Measurements for Power Systems (AMPS), 2013 IEEE International Workshop on , vol., no., pp.91,96, 25-27 Sept. 2013

Bibliography

[1] A. G. Phadke and J. S. Thorp, Synchronized Phasor Measurements and Their Applications. New York: Springer-Science, 2008.

[2] W. Premerlani, B. Kasztenny, and M. Adamiak, “Development and implementation of a synchrophasor estimator capable of measurements under dynamic conditions,” IEEE Trans. Power Del., vol. 23, no. 1, pp. 109–123, Jan. 2008.

[3] J. A. de la O Serna, “Dynamic phasor estimates for power system oscillations,” IEEE Trans. Instrum. Meas., vol. 56, no. 5, pp. 1648–1657, Oct. 2007.

[4] Instrument Transformers—Part l: Current Transformers, Int. Std. IEC 60044-1, 1996.

[5] Instrument Transformers Part 2: Inductive Voltage Transformers, Int. Std. IEC 60044-2, 1997.

[6] Model 1133A Operation Manual, Arbiter Systems, Paso robles, CA, Jul. 2011. [Online]. Available: http://www.arbiter.com/files/productattachments/133a_manual.pdf

[7] Model 1133A Phasor Measurement Specifications, Arbiter Systems,Paso robles, CA, Feb. 2007. [Online]. Available: http://www.arbiter.com/files/product-attachments/ 1133 phasor measurement specifications.pdf

[8] M. Lixia, N. Locci, C. Muscas, and S. Sulis, “Synchrophasors measurement in a GPS-IEEE 1588 hybrid system,” Eur. Trans. Elect. Power,vol. 21, no. 4, pp. 1509–1520, May 2011.

[9] P. Ferrari, A. Flammini, S. Rinaldi, A. Bondavalli, and F. Brancati, “Evaluation of timestamping uncertainty in a software-based IEEE1588 implementation,” in Proc. IEEE I2MTC, May 2011, pp. 1–6.

[10] M. Lixia, A. Benigni, A. Flammini, C. Muscas, F. Ponci, and A. Monti, “A software-only PTP synchronization for power system state estimation with PMUs,” in Proc. IEEE I2MTC, May 2011, pp. 1–6.

[11] P. Castello, M. Lixia, and C. Muscas, “Measurement of synchrophasors under dynamic conditions,” in Proc. IEEE Int. Workshop AMPS, Sep. 2010, pp. 1–6.

[12] P. Castello, C. Muscas, and P. A. Pegoraro, “Performance comparison of algorithms for synchrophasors measurements under dynamic conditions,” in Proc. IEEE Int. Workshop AMPS, Sep. 2011, pp. 25–30.

[13] Barchi, G.; Petri, D., "An improved dynamic synchrophasor estimator," Energy Conference and Exhibition (ENERGYCON), 2012 IEEE International , vol., no., pp.812,817, 9-12 Sept. 2012

[14] Belega, D.; Petri, D., “Accuracy Analysis of the Multicycle Synchrophasor Estimator Provided by the Interpolated DFT Algorithm”, IEEE Transactions on Instrumentation and Measurement, Vol. 62, Issue 5, May: 2013, pp. 942-953.

[15] Paolone, M., A. Borghetti, and C. A. Nucci. "A synchrophasor estimation algorithm for the monitoring of active distribution networks in steady state and transient conditions." Proc. of the 17th Power Systems Computation Conference (PSCC 2011), Stockholm, Sweden. 2011.

[16] Yuan-zhang, WANG Mao-hai SUN. "A DFT-based Method for Phasor and Power Measurement in Power Systems [J]." Automation of Electric Power Systems 2 (2005): 005.

[17] Karimi-Ghartemani, Masoud, Boon-Teck Ooi, and Alireza Bakhshai. "Application of enhanced phase-locked loop system to the computation of synchrophasors." Power Delivery, IEEE Transactions on 26.1 (2011): 22-32.

[18] Arnold, Jack, et al. "An Interpolated-DFT Synchrophasor Estimation Algorithm and Its Implementation in an FPGA-based PMU Prototype." Proceedings of the 2013 IEEE Power & Energy Society General Meeting. No. EPFL-CONF-188264. IEEE, 2013.

[19] Das, Sarasij, and Tarlochan Sidhu. "A Simple Synchrophasor Estimation Algorithm Considering IEEE Standard C37. 118.1-2011 and Protection Requirements." (2013): 1-1.

[20] de la O Serna, José Antonio. "Synchrophasor Estimation Using Prony's Method." Instrumentation and Measurement, IEEE Transactions on 62.8 (2013): 2119-2128.

[21] Voltage Characteristics of Electricity Supplied by Public Distribution Networks, Std. EN 50160 CENELEC, 2004.

[22] P. Kundur, J. Paserba, V. Ajjarapu, G. Andersson, A. Bose, C. Canizares, N. Hatziargyriou, D. Hill, A. Stankovic, C. Taylor, T. Van Cutsem, and V. Vittal, “Definition and classification of power system stability IEEE/CIGRE joint task force on stability terms and definitions,” IEEE Trans. Power Syst., vol. 19, no. 3, pp. 1387–1401, Aug. 2004.

[23] Electromagnetic Environment for Low-Frequency Conduced Disturbances and Signaling in Public Power Supply System, IEC Standard 61000-2-1, 1990.

[24] E. W. Gunther, “Interharmonics in power systems,” in Proc. Power Eng. Soc. Summer Meeting, 2001, vol. 2, pp. 813–817.

[25] A. G. Phadke and B. Kasztenny, “Synchronized phasor and frequency measurement under transient conditions,” IEEE Trans. Power Del., vol. 24, no. 1, pp. 89–95, Jan. 2009.

[26] IEEE Standard for Synchrophasor Measurements for Power Systems, IEEE Std C37.118.1-2011, Dec. 2011.

[27] R. K. Mai, Z. Y. He, L. Fu, B. Kirby, and Z. Q. Bo, “A dynamic synchrophasor estimation algorithm for online application,” IEEE Trans. Power Del., vol. 25, no. 2, pp. 570–578, Apr. 2010

[28] S. Huang, R. Song, and X. Zhou, “Analysis of balanced and unbalanced faults in power systems using dynamic phasors,” in Proc. PowerCon, Oct. 2002, vol. 3, pp. 1550–1557.

[29] M. A. Platas-Garza and J. A. de la O Serna, “Dynamic phasor and frequency estimates through maximally flat differentiators,” IEEE Trans. Instrum. Meas., vol. 59, no. 7, pp. 1803–1811, Jul. 2010.

[30] Voltage Characteristics of Electricity Supplied by Public Distribution Systems, Eur. Std. EN 50160, 1999.

[31] A. B. Carlson, P. B. Crilly, and J. C. Rutledge, Communication Systems: An Introduction to Signal and Noise in Electrical Communication. New York: McGraw-Hill, 2002.

[32] W. Premerlani, B. Kasztenny, and M. Adamiak, “Development and implementation of a synchrophasor estimator capable of measurements under dynamic conditions,” IEEE Trans. Power Del., vol. 23, no. 1, p.109–123, Jan. 2008.

[33] R. K. Mai, Z. Y. He, L. Fu, B. Kirby, and Z. Q. Bo, “A dynamic synchrophasor estimation algorithm for online application,” IEEE Trans. Power Del., vol. 25, no. 2, pp. 570–578, Apr. 2010.

[34] Roscoe, A. J., I. F. Abdulhadi, and G. M. Burt. “P and M Class Phasor Measurement Unit Algorithms using Adaptive Cascaded Filters.”, available on line.

[35] Moraes, R.M.; Yi Hu; Stenbakken, G.; Martin, K.; Alves, J.E.R.; Phadke, A.G.; Volskis, H.A.R.; Centeno, V., “PMU Interoperability, Steady-State and Dynamic Performance Tests,” Smart Grid, IEEE Transactions on , vol.3, no.4, pp.1660,1669, Dec. 2012

[36] IEC Communication networks and systems for power utility automation,IEC 61850 Ed. 2, 2011.

[37] Apostolov, A.; Vandiver, B.; , "IEC 61850 process bus - principles, applications and benefits," Protective Relay Engineers, 2010 63rd Annual Conference for , vol., no., pp.1-6, March 29 2010-April 1 2010

[38] Martin, K.E.; , "Synchrophasor Standards Development - IEEE C37.118 & IEC 61850," System Sciences (HICSS), 2011 44th Hawaii International Conference on , vol., no., pp.1-8, 4-7 Jan. 2011.

[39] Kezunovic, M.; , "Verifying interoperability and application performance of PMUs and PMU-enabled IEDs at the device and system level,"Innovative Smart Grid Technologies (ISGT), 2012 IEEE PES, vol., no., pp.1-3, 16-20 Jan. 2012.

[40] Castello, P.; Ferrari, P.; Flammini, A.; Muscas, C.; Rinaldi, S.; , "An IEC 61850-Compliant distributed PMU for electrical substations," Applied Measurements for Power Systems (AMPS), 2012 IEEE International Workshop on , vol., no., pp.1-6, 26-28 Sept. 2012.

[41] Ingram, D.M.E.; Campbell, D.A.; Schaub, P.; Ledwich, G.; , "Test and evaluation system for multi-protocol sampled value protection schemes," PowerTech, 2011 IEEE Trondheim , vol., no., pp.1-7, 19-23 June 2011.

[42] IEEE 1588-2008, IEEE Standard for Precision Clock Synchronization Protocol for Networked Measurement and Control Systems, July 2008.

[43] IEEE Standard Profile for Use of IEEE 1588 Precision Time Protocol in Power System Applications, IEEE Std C37.238-2011, pp.1-66, 2011.

[44] UCA International Users Group: Implementation Guideline For Digital Interface to Instrument Transformers Using IEC 61850-9-2.

[45] PTPd Daemon Project. Available on line: http://ptpd.sourceforge.net/.

[46] Ferrari, P.; Flammini, A.; Rinaldi, S.; Prytz, G., "Evaluation of Time Gateways for Synchronization of Substation Automation Systems," Instrumentation and Measurement, IEEE Transactions on , vol.61, no.10, pp.2612,2621, Oct. 2012.

[47] De Dominicis, C.M.; Ferrari, P.; Flammini, A.; Rinaldi, S.; Quarantelli, M., "On the Use of IEEE 1588 in Existing IEC 61850-Based SASs: Current Behavior and Future Challenges," Instrumentation and Measurement, IEEE Transactions on , vol.60, no.9, pp.3070,3081, Sept. 2011.

[48] AD 7656 Datasheet. Available online at: www.analog.com.

[49] Liu, J., Ni, F., Pegoraro, P. A., Ponci, F., Monti, A., & Muscas, C. (2012, September). Fundamental and harmonic synchrophasors estimation using modified Taylor-Kaiman filter. In *Applied Measurements for Power Systems (AMPS), 2012 IEEE International Workshop on* (pp. 1-6). IEEE.

Acknowledgements

Questo lavoro di tesi è il completamento di tre anni di studio, un traguardo che ho il piacere di condividere con diverse persone importanti e che, in modi diversi, hanno contribuito affinché completassi questo percorso. La lista è lunga e sicuramente non potrò ringraziarle tutte.

Il mio primo ringraziamento va a Carlo, il mio tutor di dottorato e relatore di due tesi di laurea che mi ha guidato nel mondo della ricerca e mi ha formato come ingegnere.

Durante questi tre anni ho avuto la fortuna di poter lavorare con Paolo che ha sempre supervisionato i miei lavori aiutandomi a dare il meglio.

Ringrazio Sara che mi ha sempre sostenuto con i suoi preziosi consigli in questi tre anni di dottorato.

Ringrazio i Professori Antonello Monti e Ferdinanda Ponci, Junqi Liu e tutti gli amici di Aachen per l'inteso e proficuo periodo trascorso in Germania. Ringrazio Stefano Rinaldi e gli amici dell'Università di Brescia per la preziosa collaborazione che ha arricchito questo lavoro di tesi.

Un ringraziamento speciale ai miei compagni di percorso, Marco e Marco con cui ho passato giornate indimenticabili durante i "Gorini" e con cui ho condiviso momenti belli e impegnativi.

Ringrazio la mia famiglia, lo zio Paolo, la zia Lena e tutti gli amici di Caravaggio senza i quali non avrei mai potuto raggiungere i traguardi di questi anni.

Voglio ringraziare gli studenti a cui ho supervisionato le tesi di laurea e gli studenti dei corsi di cui sono stato tutor: mi avete permesso di mettermi sempre gioco e a non dare mai nulla per scontato con le vostre domande mai banali.

Ringrazio i miei amici a cui ho tante volte ho detto "no" ma che hanno sempre capito che lo facevo per passione, anche quando la stanchezza e la pazienza erano finite. Tra questi un ringraziamento speciale a Giuseppe, Alessio, Caterina, Elisabetta, Carla, Valentina, Ignazio, Carlo e Marco. Grazie mille ai colleghi di dottorato e a tutti gli abitanti del seminterrato che mi hanno fatto passare tanti momenti divertenti quando ce n'era davvero bisogno.

Un grazie a Simona, arrivata giusto in tempo per meritarsi un ringraziamento speciale per avermi sostenuto dalla prima riga di questa tesi.

List of figures

Figure 1. Standalone PMU device from Arbiter, model 1133A power sentinel 13
Figure 2. block diagram of a stand alone PMU 14
Figure 3. Convention for synchrophasor representation 17
Figure 4. Sinusoid with a frequency $f>f_o$ observed at instants that are multiples of T_0 18
Figure 5. The TVE criterion shown on the end of phasor 20
Figure 6. TVE % as a function of magnitude for various phase errors 20
Figure 7. TVE as a function of phase for various magnitude errors 21
Figure 8 Example of a step change measurement with all the indices for this test. Step at t=0. 22
Figure 9. Frequency step test phase response without group delay compensation. Step at *t=0* 23
Figure 10. Out of band interference area for a reporting rate equal to 50 Fs 26
Figure 11. Spectrum of an amplitude-modulated signal 34
Figure 12. Qualitative behaviour of dynamic phasor model in the frequency domain 35
Figure 13. The number of cycles used from each algorithms 40
Figure 14. TVE % results for off-nominal frequency f=52.5 Hz 43
Figure 15. Maximum amplitude error (%) and phase error (crad) for the tests in presence of harmonics for different frequencies 44
Figure 16. Maximum TVE % in presence of a single interharmonic at frequency f_i 45
Figure 17. TVE trends for the -20 % magnitude step test 48
Figure 18. Flux diagram of the modified method 54
Figure 19. Maximum and mean TVE (%) values for an amplitude modulation test 55
Figure 20. TVE response time for an amplitude step test of +20% 56
Figure 21. Δt_R for H_T = 1% for a positive phase steps from +5° to +90° 57
Figure 22. TVE response time for an phase step test of +45° 57
Figure 23. Diagram of the proposed solution 59
Figure 24. Frequency feedback area 60
Figure 25. Steady state compliance test for harmonic rejection. 62
Figure 26. Steady state compliance test for out of band interfering signals. 63
Figure 27. Dynamic compliance test for modulated signals and frequency ramp 64
Figure 28. The scheme of the CompactRIO device from National Instruments 68
Figure 29. Scheme of the PMU prototype 69
Figure 30. Data set of the acquired signal. 70
Figure 31. The communication system of the PMU prototype 71
Figure 32. Data Dashboard from National Instruments to receive the shared variables from the PMU prototype. 72
Figure 33. User interface software to control the PMU prototype 72

Figure 34. The PMU prototype under the synchronization test with different signals..... 73
Figure 35. The proposed distributed measurement architecture based on IEC 61850 78
Figure 36. The architecture of IEEE 1588 Merging Unit Prototype 79
Figure 37. The experimental set-up adopted to evaluate synchronization performance of MUs 80
Figure 38. The distribution of the time offset between the IEEE 1588 MUs (54000 samples)..... 80
Figure 39. The second experimental set-up adopted to evaluate synchronization performance of MUs 81
Figure 40. The distribution of phase error of the sampling signals generated by synchronized MU prototypes (1000000 samples)..... 82
Figure 41. The distribution of the frequency ratio of sampling signals generated by two synchronized MUs 82
Figure 42. Test with off-nominal frequency: signal frequency range for M class and TVE % (limit 1 %) 83

List of tables

Table 1. Required PMU reporting rate 13

Table 2. Measurement reporting latency 24

Table 3. Steady state synchrophasor, frequency and ROCOF measurement requirements for a reporting rate Fs ≥ 25 frames/s 25

Table 4. Dynamic synchrophasor, frequency and ROCOF measurement requirements for a reporting rate Fs ≥ 25 frame/s 27

Table 5. Phasor, frequency and ROCOF performance requirements for input step change for reporting rate from 25 up to 50 frame/s 28

Table 6. Maximum TVE % results for 55 Hz Harmonic Test 44

Table 7. Maximum amplitude and phase error for amplitude modulated signal (kx=0.1 and fm = 5Hz) 46

Table 8. Maximum amplitude and phase error for amplitude and phase modulated signal (kx,ka = 0.1 and fm = 5Hz) 47

Table 9. Maximum module and phase results for ramp test for ramp test with ROCOF = 1 Hz/s 47

Table 10. Δt_r values for Ht = 1% and Ht = 3% in the -20 % amplitude step test 49

Table 11. Summary of method performances 49

Table 12. Δt_r values for Ht = 1% and Ht = 3% for a +20% and a +10% amplitude step test 56

Table 13. t_r results for tests in presence of step changes and harmonics at off-nominal frequency equal to 52.5 Hz. 58

Table 14. tr values for tests where a step change and harmonics are superimposed on amplitude and phase modulation at off-nominal frequency equal to 52.5 Hz. 58

Table 15. Steady State Compliance Tests for Off-nominal frequency 61

Table 16. Steady State Frequency Compliance Test for P Class 63

Table 17. Steady State ROCOF Compliance Test for P Class 63

Table 18. Frequency Estimation under Modulated Signal and Frequency Ramp Tests for P Class 65

Table 19. ROCOF Estimation under Modulated Signal and Frequency Ramp Tests for P Class 65

Table 20. Synchrophasor Estimation under Step Change Test for P Class 65

Table 21. Frequency estimation under Step Change Test for P Class 66

Table 22. ROCOF estimation under Step Change Test for P Class 66

Table 23. PMU Tests: summary of compliance 67

Table 24. Maximum TVE % for harmonic distortion tests (limit 1 %) 84

Table 25. Maximum TVE % for out-of-band interference tests for reporting rate equal to 50 (limit 1.3 %) . 84

Table 26. Maximum TVE % for frequency ramp tests with rate ±1 Hz/s (limit 1 %) 84

Table 27. Maximum TVE % for amplitude and phase modulation tests (limit 3 %) 85

Table 28. Response time for amplitude and phase step tests 85

Table 29 Latency requirements for P and M class for the different Reporting Rate 86